2016-08-01

Packing Sheet Materials Into Cylinders and Prisms Using Origami-based Approaches

Jared Thomas Bruton
Brigham Young University

Packing Sheet Materials into Cylinders and Prisms Using Origami-Based Approaches

Jared Thomas Bruton

A thesis submitted to the faculty of
Brigham Young University
in partial fulfillment of the requirements for the degree of

Master of Science

Spencer P. Magleby, Chair
Larry L. Howell
John L. Salmon

Department of Mechanical Engineering

Brigham Young University

August 2016

ABSTRACT

Packing Sheet Materials into Cylinders and Prisms Using Origami-Based Approaches

Jared Thomas Bruton
Department of Mechanical Engineering, BYU
Master of Science

Packing sheet materials into cylinders and prisms using Origami-based approaches (Soft Origami or traditional Origami) is of interest in fields where sheet materials need folded into cylinders or prisms. Fully-dense packing has application in fields where a sheet material is to be folded with minimal gaps into a cylinder or prism. Partially-dense packing is applicable to fields where gaps are required between packed surfaces or where hollow volumes are to be filled, such as in fluid filter design.

Soft Origami is explored as a method for folding soft-sheet materials into fully-dense cylinders. Two fold patterns, the "flasher" and the "inverted-cone fold," are explored for packing soft-sheet materials into cylindricals. An application to driver's side automobile airbags is successfully performed, and deployment tests are completed to compare the influence of packing method and origami pattern on deployment performance. In total, two origami patterns and six packing methods are examined for folding soft-sheet materials into fully-dense cylindrical prisms, and it is shown that modifying the packing method impacts deployment performance.

A special case of the Miura-ori, the ninety-degree case, is briefly explored as a traditional Origami method for packing arbitrary-shaped sheet materials into fully-dense arbitrary prisms. Examples are shown and it is concluded that this pattern can be used to configure a large number of fully-dense packed prisms with configurable characteristics.

Finally, patterns that fold into partially-dense cylindrical prisms are examined using traditional Origami approaches and their efficiency compared. Efficiency is defined as the ratio of the surface area of a pattern compared to an idealized high-surface-area model. Patterns include traditional (non-Origami-based) fluid filter patterns (the Basic Pleat and M-pleat) and cylindrical Origami patterns (the Accordion and Kresling). An offset crease method is used to modify the Accordion and Kresling Origami patterns so the comparison is objective. Results are presented that determine which individual pattern variations have the highest efficiency at different outside-to-inside diameter ratios. Ranges over which each pattern is most efficient are presented. It is concluded that based purely on geometry, the M-pleat provides the highest overall efficiency, but depending on other factors each pattern is viable for different purposes.

Keywords: Soft Origami, cylinder, airbag, prism, packing efficiency, fluid filter

ACKNOWLEDGMENTS

I would like to thank my wife Ariel and daughter Vivian for providing help and motivation throughout my research. I would also like to thank my siblings, parents (Tom and Cindy Bruton), in-laws (Rod and Marsha Jay), sibling-in-laws, and numerous neices and nephews, all for being interested in and supportive of my research.

I thank Dr. Spencer Magleby, Dr. Larry Howell, and Dr. John Salmon for their help and support throughout and for providing feedback and advice both about research and life. Particularly, I thank Dr. Magleby for being supportive of my research and my personal life, and for providing an always-optimistic outlook on research and life, and Dr. Howell for providing many pieces of professional advice.

I could not have accomplished this work without much help from other students in our research group. I thank Todd Nelson, Jason Dearden, Michael Morgan, Kyler Tolman, Trent Zimmerman, Jason Lund, Jared Butler, and Ezekiel Merriam for help on code, geometry, writing, and for sharing many positive experiences both inside and outside research and classes.

For the research in Chapter 2, I thank my co-authors Todd Nelson, Trent Zimmerman, Janette Fernelius, Larry Howell, and Spencer Magleby for assisting in various and difficult portions of the research. I gratefully acknowledge Bryce Hansen for helping with paper graphics, Quin Soderquist and technicians and collaborators at Autoliv who conducted deployment tests, analysis, and provided technical feedback, Sarah Shipp for assistance in folding final prototypes, Matthew Gong and Peter Schleede for mathematical and conceptual assistance, Katherine Jensen for help with prototyping.

For the research in Chapter 3, I thank Mary Wilson for designing and creating the thick Miura-map model shown in Fig. 3.2 and granting permission to photograph and use photos of it.

For the research in Chapter 4, I thank my co-authors Bridget Beatson, Matthew Gong, Larry Howell, and Spencer Magleby for helping perform the research throughout the process. I also thank Terri Bateman for help throughout the project and many valuable pieces of advice about project management. I acknowledge Cummins Filtration for providing in-kind support of fluid filter material and existing fluid filters for comparison. I thank Sara Shipp for aid folding prototypes, and Peter Schleede and Kyler Tolman for mathematical and conceptual assistance throughout the project. I thank Dr. Robert Lang of Lang Origami for helping modify the Accordion and Kresling patterns and also providing valuable literature references.

This material is based upon work supported by the National Science Foundation and the Air Force Office of Scientific Research, NSF Grant No. EFRI-ODISSEI-1240417 and National Science Foundation Graduate Research Fellowship Program under Grant No. 1247046. In-kind support of airbag supplies and testing facilities and support was provided by Autoliv, and in-kind support of fluid filter material and existing fluid filters for comparison was provided by Cummins Filtration.

TABLE OF CONTENTS

LIST OF TABLES

LIST OF FIGURES

CHAPTER 1. INTRODUCTION

1.1 Motivation

Packing sheet materials into cylinders and prisms using Origami-based approaches (Soft Origami or traditional Origami) is of interest in fields where sheet materials need folded into cylinders or prisms. These cylinders or prisms may be either fully-dense or partially dense depending on application. A fully-dense cylinder is shown in Fig. 1.1(a) and a partially-dense (hollow) cylinder is shown in Fig. 1.1(b). A fully-dense arbitrary prism is shown in Fig. 1.2(a) and a partially-dense arbitrary prism is shown in Fig. 1.2(b).

Fully-dense packing has applications in fields where a sheet material is to be folded with minimal gaps (no internal cavities) into a cylinder or prism. Fully-dense cylindrical packing has application in fields such as parachute packing, tent packing, and airbag packing where a soft-sheet material is packed into a cylindrical container. Fully-dense prism packing has application in fields where a sheet material is to be folded with minimal gaps into a prismatic shape, including possible application to the same fields such as parachute packing, tent packing, and airbag packing if reconfigurable packing and specific shape-matching is of interest (i.e. stowing these items in non-cylindrical containers). Partially-dense packing has application in fields where a sheet material is to be folded into a shape with openings, channels, or gaps for applications such as fluid flow. Partially-dense cylindrical packing is applicable to fields where flow is required such as in fluid filter design. Partially-dense prism packing, while mentioned in Chapter 3, is not explored in depth in this thesis.

Previous work has been done in both topics (cylinder and prism packing) primarily from an industry perspective. However, approaching the design challenges inherent in these topics from an Origami-based perspective (both Soft Origami and traditional Origami) is a valuable addition in this field, and this thesis seeks to expand the Origami-based design processes relating to this topic.

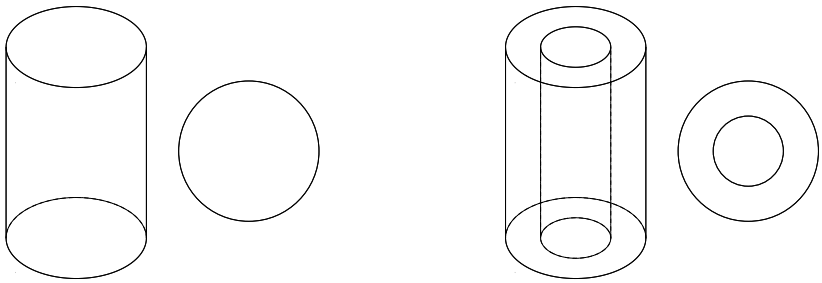

(a) (b)

Figure 1.1: (a) Fully-dense cylinder (b) partially-dense cylinder.

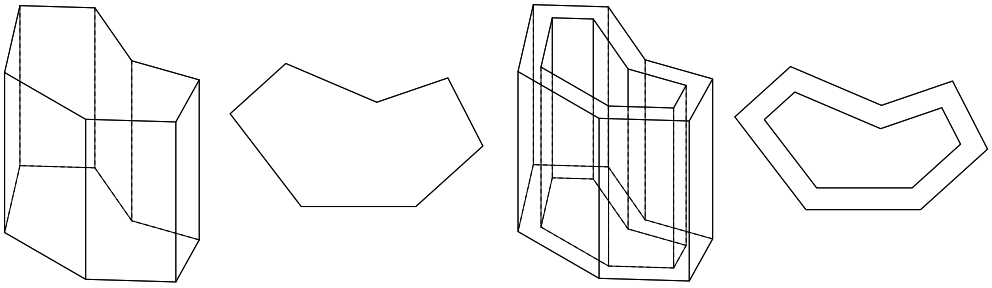

(a) (b)

Figure 1.2: (a) Fully-dense arbitrary prism (b) partially-dense arbitrary prism.

1.2 Objective

The objective of this research is to show methods and metrics that help designers use innovative Origami-based folding methods to achieve various objectives associated with sheet-material packing. Methods for packing soft-sheet materials into fully-dense packed cylinders using Soft Origami will be considered. A method for packing sheet materials into fully-dense arbitrary prismatic shapes using traditional Origami is considered. Finally, methods for designing and metrics for comparing cylindrical partially-dense packing patterns using traditional Origami are to be developed. Through application to fields of interest including automotive airbags and fluid filters, the impact of original pattern design and folding and packing methods on performance is considered.

1.3 Thesis Outline

The approach taken in this thesis focuses on subdividing cylinder and prism packing into fully-dense and partially-dense categories and exploring each in turn.

Chapter 1 introduces the topic, objective, and motivation behind the research.

Chapter 2 explores configurable packing of fully-dense cylinders with Soft Origami. Such packing is useful for applications where a soft-sheet material needs packed into a cylindrical container or volume. Through application to automobile airbags, the effect of both original pattern and packing method on both stowed position characteristics and deployment characteristics are examined. This chapter has been submitted for publication in the Royal Society Open Science journal.

Chapter 3 explores configurable packing of fully-dense arbitrary prisms using traditional Origami. A special case of the Miura-ori, the ninety-degree Miura-ori, is used to show one potential method for packing materials into arbitrary-shaped prisms. Another consideration addressed in brief is that of arbitrary-shaped sheet materials, and the ability to fold a continuous arbitrary-shaped sheet into arbitrary prismatic shapes.

Chapter 4 explores configurable packing of partially-dense (hollow and with gaps between folded surfaces) cylindrical patterns from a traditional Origami perspective. A method of comparison between different patterns is shown, and application to fluid filters is considered. Optimal values for designing such cylindrical patterns are considered. This chapter will be submitted for publication in the International Journal of Mechanical Sciences.

Chapter 5 presents conclusions drawn from the research and areas of possible future work.

CHAPTER 2. PACKING AND DEPLOYING SOFT ORIGAMI TO AND FROM CYLINDRICAL VOLUMES WITH APPLICATION TO AUTOMOTIVE AIRBAGS

2.1 Introduction and background

Packing and deployment of Soft Origami (soft-sheet materials folded into origami patterns) to and from cylindrical volumes is of interest in industries where a flexible sheet of material needs to fit into a confined cylindrical shape prior to being deployed via mechanisms or internal pressure.

For the purpose of this research, soft-sheet material is defined as material of constant thickness with approximately zero stiffness (for example textiles, fabrics, and thin-sheet polymers). Soft-sheet materials can easily wrinkle, bend, and crease locally, which can be advantageous when using them with origami fold patterns.

2.1.1 Origami and engineering design

Applying patterns extracted from or inspired by origami to engineering design can inspire new approaches to design problems. Possible benefits of applying origami to engineering design include predictable deployment, compact packing, and a large number of available patterns. Previous research has explored rigid-foldable pattern applications and methods for applying origami patterns to materials thicker than paper [1–3], the use of flasher patterns for space applications [4], design of developable surfaces and other patterns based on curved-crease origami [5–7], use of computational methods to design complex fold patterns and shapes [8, 9], and general methods for selecting origami patterns and applying them to design problems [10].

Another topic that has been considered in origami and engineering is that of scalable and easily configurable packing and pattern design. If designers need to fit a common pattern

(which may be scaled proportionately larger or smaller) into a specific container or packed shape, this characteristic is particularly valuable, and origami provides a method for creating such scalable designs. Examples of scalable packing and pattern design within the realm of cylindrical designs include deployable solar arrays [4], heart stents [11], and a heart structure support system for patients experiencing heart failure [12].

2.1.2 Soft Origami and use of soft-sheet materials

Use of soft-sheet materials with origami patterns falls under the umbrella of "Soft Origami" based on a qualitative understanding of the compliance of the soft-sheet materials being used with origami patterns. Soft Origami has recently been explored as a method for applying origami design methods to flexible materials or substrates, with potential applications in bio-engineering (e.g. 3D tissue scaffolding), flexible electronics, and other applications where highly compliant hinges are required or useful and it is desirable to impose an origami pattern using negligible force [13]. Using origami patterns is a valuable approach due to the ability to pack soft-sheet materials into a desired packed position and subsequently deploy them from that position. Because soft-sheet materials are extremely compliant and can wrinkle, bend and crease locally to accommodate for inexact folding of the origami pattern fold lines, no strictly defined fold lines or "hinges" are needed, which simplifies manufacturing. Soft Origami yields possible benefits in fields including airbag manufacturing and packing, air filter design and manufacture, parachute packing and deployment, deployable inflated structure design (including inflatable space habitats such as the BEAM module installed in 2016 on the International Space Station [14–17]), inflatable watercraft, inflatable personal amusement equipment, bounce houses, slides, and hot air balloons), tent packing, umbrella packing and deployment, shade covers (e.g. track tents), and emergency blanket packing.

Deployment performance also requires consideration when applying Soft Origami to design problems. In some cases deployment will happen many times throughout the lifetime of the product (e.g. a camping tent) and in others deployment will happen only once (e.g. automotive airbags). Depending on how critical repeat deployment performance is, different levels of care need to be taken when selecting packing patterns. In cases such as

automotive airbags and parachutes where human life is dependent on the accurate unfolding of the structure, extensive testing and refinement is key to ensure that the final deployment performance meets required standards. In other cases, many different patterns may be used to accomplish the same purpose so long as the final packed product fits in the required space or package (e.g. tent in a tent bag, umbrella in a storage bag, emergency blanket in a storage package). In applications where deployment occurs via a pressure differential (e.g. being filled with air or another gas) and where the products cannot have rigid items inside them for safety reasons (e.g. airbags), a crucial requirement which Soft Origami and soft-sheet materials can meet is a packing method wherein any rigid members used in the folding process are removed before the product is functional or deploys. This allows the design of an intentional deployment sequence (via the imposed origami pattern) while not requiring dangerous internal rigid mechanisms inside the product, and adds to the benefits of using Soft Origami and soft-sheet materials.

2.1.3 Objective

In this research, fold patterns and packing methods are considered that efficiently pack soft-sheet materials using Soft Origami techniques into cylindrical packed shapes with configurable folded (packed) height and diameter, deployed (unfolded) shape, and deployed size. Deployment performance and the impact of packing method on deployment are also explored. Two fold patterns and associated packing methods each are investigated as potential solutions for packing a soft-sheet material into a desired cylindrical shape. As a demonstration, these patterns and packing methods are applied to an automotive airbag case study, and deployment performance considered and compared.

2.2 Cylindrical Packing And Deployment

One common current method used to pack a soft-sheet material into a cylinder is to directly compress the soft-sheet material into the desired packed shape and container without specific fold patterns (similar to how a sleeping bag is often forced into a cylindrical "stuff sack"). However, this technique can lead to unpredictability in deployment. Depend-

Figure 2.1: An undeployed flasher pattern with cylindrical envelope shown around it. Specified height H and diameter D are variables of interest.

ing on the application, this may or may not be acceptable. Other basic fold patterns exist (such as the "tri-fold" method commonly used to fold tents where the object is folded like a tri-fold brochure prior to rolling the material up into a tightly-packed cylinder) which may be sufficient depending on the application. This research proposes two origami patterns that can be applied to soft-sheet materials to achieve a similar packed shape and size while allowing for different deployment performance, and it is shown that specific desired deployment characteristics can be dictated by modifying packing (folding) methods.

The desired parameters for the final packed shape are the diameter D and height H of a cylinder circumscribed around the folded pattern, shown in Figure 2.1. In the following subsections, our pattern selection, packing methods, and deployment considerations are presented. Origami patterns are used in this research as a mechanism to generally predict packed shape and deployment characteristics.

2.2.1 Pattern selection and modelling

A search of origami patterns was conducted with a focus on finding patterns that fold into a generally cylindrical shape and can be mathematically modelled and modified. These patterns included a six-sided origami flasher model, Miura, Arc-Miura and tapered

Miura [18], cylindrical Kresling pattern [19], waterbomb magic ball [20], and the fold pattern of a collapsible umbrella.

Several of these patterns do not scale well to different heights. That is, some of the patterns (such as the arc-Miura) do not contract in both directions (radially and axially) when deployed. For these patterns, if the deployed structure has to be a certain packed height, the packed height is the same as the height of the deployed pattern. As a result, patterns that do not scale well to different packed heights (e.g. the Miura and derivatives) were not selected for this research.

Two patterns were selected based on their reconfigurability and ability to pack closely into a cylinder: the flasher pattern and the "umbrella fold" pattern. The flasher pattern, shown in Fig. 2.2, is desirable due to its scalable height and deployed surface area, shape, and size. Because there exist rigid-foldable versions of the flasher [21], we can create a method using rigid panel folding devices to fold a soft-sheet material into a tightly packed cylinder with the ability to select specific dimensions such as packed height and unfolded diameter. The "umbrella fold," also desirable for its scalable height and configurable deployed surface area and shape, is a soft-sheet material approximation of a developable surface curved-crease pattern, the cone inversion [5, 22], shown in Fig. 2.3. The developable cone inversion that exists in the umbrella fold is shown in Fig. 2.3(b) along with a semi-transparent overlay of a generic umbrella. This pattern, or variations of it, has been previously used in art pieces [23]. In particular, this is a simple version of a developable surface pattern wherein a cone is inverted several times between the peak and the base. To distinguish this particular pattern from other patterns that are used to fold umbrellas, this pattern (when folded in soft-sheet materials) will be referred to as the "inverted-cone fold." The curved crease version shown in Fig. 2.3(a) has some final angle between inverted layers and cannot compress into a cylinder as a result. Using soft-sheet materials enables us to compress the pattern past the curved crease version's final angle into a compact cylinder.

The selected patterns both allow for reconfigurable surface area, size and shape, and packed height. By changing selected parameters of each pattern, a near-infinite number of variations can be created that pack and deploy in the desired fashion. When these patterns are imposed on soft-sheet materials, the materials can be compressed into an approximately

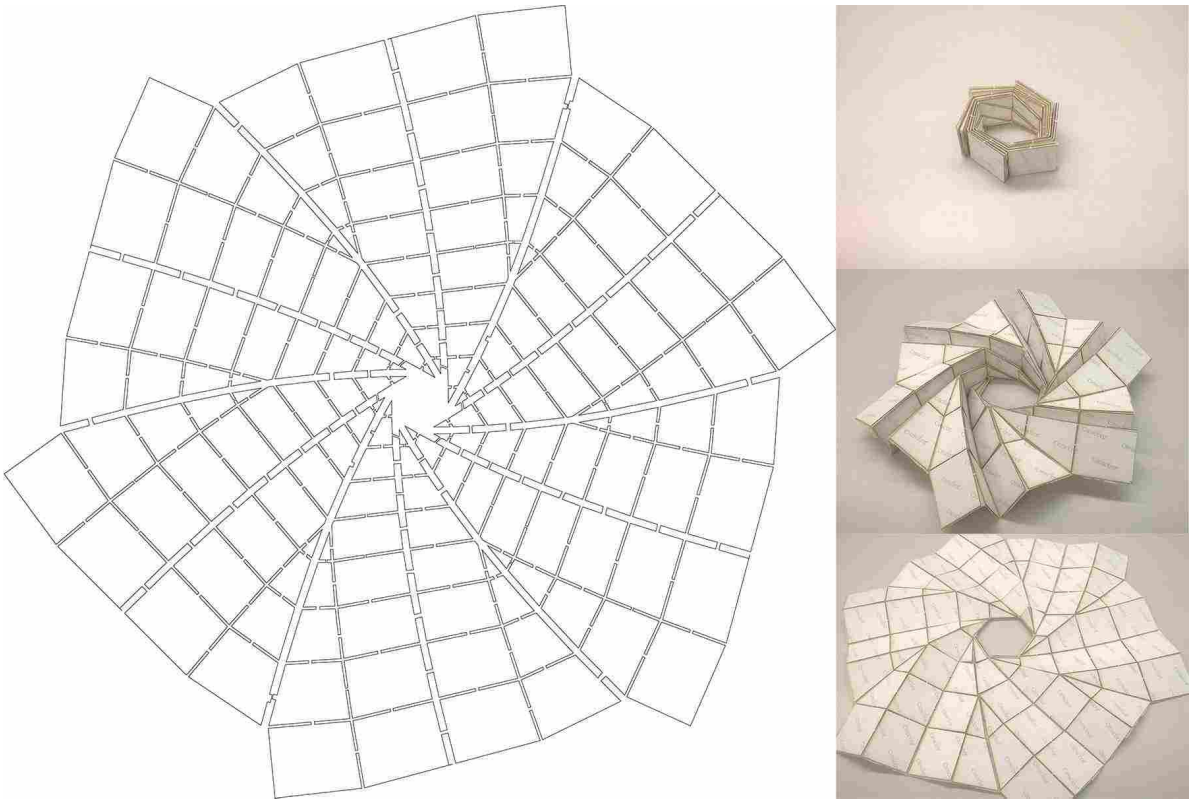

Figure 2.2: Flasher flat pattern (left) and matboard physical prototype with plastic backing hinge layer, in various stages of deployment (right).

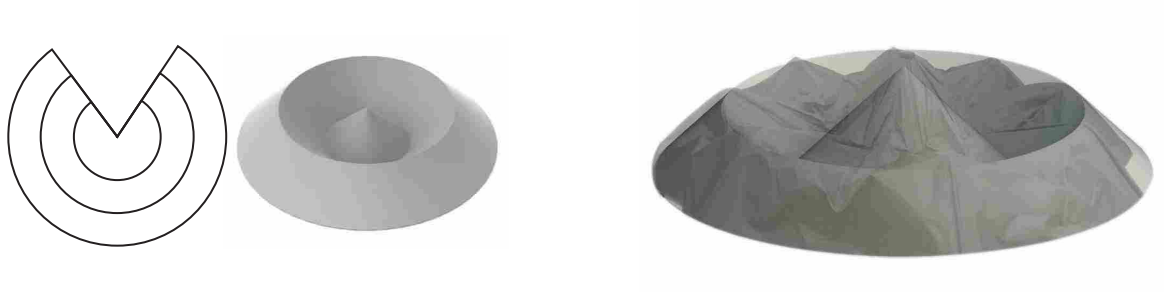

(a) (b)

Figure 2.3: Inverted-cone fold (a) curved-crease origami pattern and 3D model of folded pattern (b) umbrella photo overlaid on inverted-cone fold shape.

cylindrical packed shape. This feature is the most important factor used in selection of these two patterns for pursuing further. In the following section potential manufacturing (packing) methods for applying both patterns to soft-sheet materials are explored.

2.2.2 Packing Methods

Packing methods were constructed to pack a soft-sheet-material into the selected patterns. In this case, origami patterns were used as inspiration for the packing methods, and the methods are effectively origami-inspired tooling for folding soft-sheet materials into the desired shape. Individual packing methods for each pattern are detailed as follows.

Flasher

The flasher fold pattern, with fold pattern and physical prototype shown in Fig. 2.2, consists of an origami pattern that can be reconfigured to pack in a shape close to a cylinder. The example used here is a hexagonal flasher with reconfigurable height and deployed shape. Although a hexagonal pattern is shown here, other polygonal shapes are also possible. This pattern has previously been applied to space solar arrays using thickness-accommodation techniques [4] and other applications where a large deployed-area-to-packed-shape is desirable. Another benefit of the flasher pattern is that the soft-sheet-material contracts equally in the radial direction at all points around the circle of material, so there are no uneven flaps left over such as occurs with a common collapsible umbrella.

One possible packing method for the flasher fold pattern is to use a flasher such as that made of matboard shown in Fig. 2.2 as a folding structure with the soft material on top of it; the material is folded into the flasher shape on top of the structure and then removed. A variation on this packing method is to use two folding tables with the material sandwiched in between. A second method would be to create a series of rigid links that are constrained to fold in the same method as the flasher.

Inverted-Cone Fold

The inverted-cone fold pattern is shown in Fig. 2.3(a). This pattern is a series of cones that have been inverted multiple times, resulting in a series of concentric rings if viewed from above, and is also referred to as a developable surface cone inversion [24]. While the pattern shown here has only one valley and one mountain fold between the central peak and the

outside edge, more rings could be added to increase the diameter of the shape. This curved-crease fold has been used for many years, particularly as art. Variations (many of which are more complex) on this pattern can be seen in Ron Resch's work entitled "Yellow Cones Kissing" as well as in multiple pieces by David Huffman such as "Cone Reflected 7 Times" and pieces by Hiroshi Ogawa [6].

If the fully-developable inverted-cone pattern is made of a soft-sheet material that can wrinkle, bend, and crease locally, this pattern is viable for making a packed cylindrical shape where the original shape, surface size, diameter, final packed height, and packed diameter are all selectable. Using material that can wrinkle, bend, and crease locally allows us to use the "skeleton" of the developable cone inversion shape to fold the fabric. A rigid link mechanism "skeleton" can be created based on the curved crease pattern which can be used to fold soft-sheet materials into a close approximation of a cylinder. The rigid mechanism used for folding can be removed prior to deployment.

Several options are viable for manufacturing or folding a soft-sheet material into the inverted-cone pattern. One method was inspired by a common mechanism used to fold collapsible umbrellas. Collapsible umbrellas typically have a series of rigid links that control the fabric (a soft-sheet material). Because the fabric can wrinkle, bend, and crease locally, the approximate cone inversion can go from fully packed to open, unlike a non-soft-sheet material version. Typically, an umbrella does not go completely flat when open (rather making a sloped shape to ensure that water runs off at the outside). The rigid links overlayed on an inverted-cone fold with two exterior rings are shown on the developable surface curved crease cone inversion in Fig. 2.4. The length of the links can be scaled to achieve a specified packed height and the number of layers dictates the deployed surface area and size. The designer can change the number of layers and layer height to achieve highly reconfigurable packed and deployed sizes. There is a trade-off between number of layers (how many rings there are viewed from the top) and packed diameter. Specifically, each ring adds at least $4t$ in overall thickness to the diameter, where t is the thickness of the material.

In the case of the umbrella, the links correspond to ruling lines inherent in a developable surface cone inversion [25]. If the number of links corresponding to ruling lines is increased to infinity, the lines would approach the form of a developable cone inversion sur-

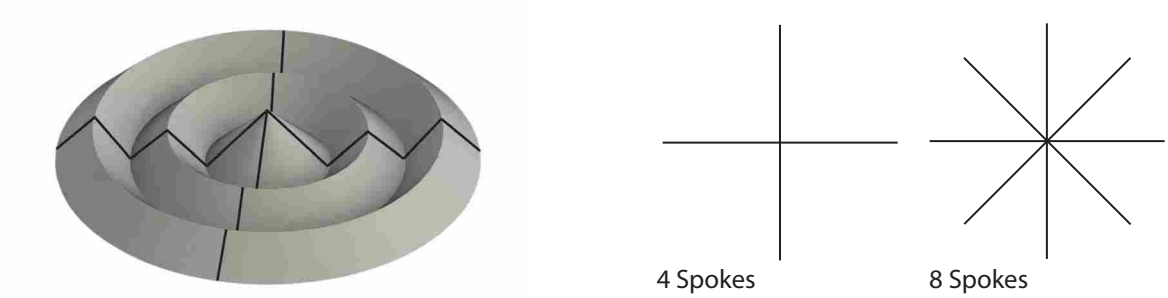

(a) (b)

Figure 2.4: Inverted-cone fold (a) rigid links (similar to an umbrella) that allow an umbrella made of extensible fabric to transition from fully open to fully closed position and (b) two different spoke configuration options.

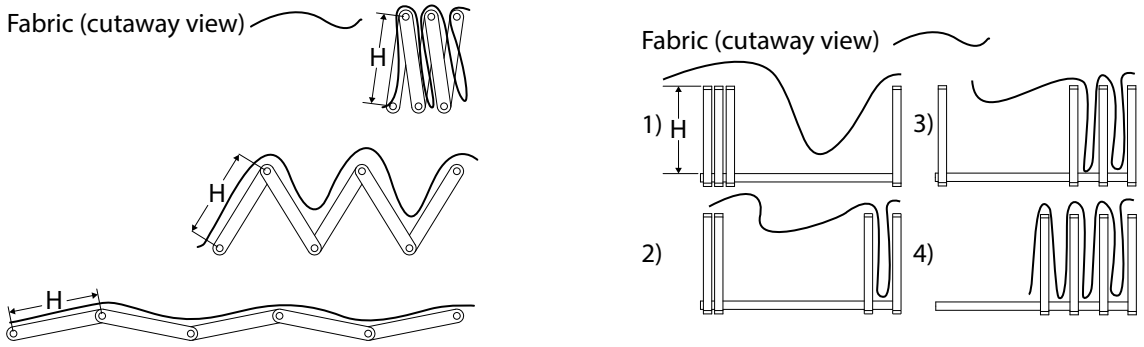

(a) (b)

Figure 2.5: Inverted-cone fold folding methods (a) linkage mechanism packing method, with fabric laid on a linkage mechanism formed of rigid links where height H of the packed pattern can be selected by choosing desired link lengths, and the mechanism can be removed from the material when folding is completed (b) slider mechanism packing method, with fabric laid on top of the slider assembly in Step 1, and folded into the layers, progressing through Step 2, Step 3, and Step 4. In both (a) and (b), the final packed height H of the mechanism is equal to the length of the links and sliders respectively.

face. However, there is a physical limit due to the size and interference of the necessary link arms. Having some evenly spaced number of "spokes" that are used as folding mechanisms is a potential manufacturing method, and more spokes may lead to a more accurate fold pattern, as shown in Fig. 2.4(b).

Using the idea of spokes, two different manufacturing methods, shown in Fig. 2.5, were investigated. Each could be done with any desired number of spokes greater than three, as

allowed by physical manufacturing limits. In physical prototypes we created, the number of spokes used was four. The first manufacturing method is to use a linkage similar to the link overlay previously shown in Fig. 2.4(a). Figure 2.5(a) details this linkage, wherein fabric is laid on top of the mechanism spokes, secured using suction or weak adhesion and the linkage then folded up. In this case, the height H of the folded pattern will be approximately equal to the length of each link. One common mechanism that could be adapted for this purpose is a scissor mechanism or linkage, which would reduce the required degrees of freedom compared to the linkage mechanism shown.

Due to the discretised manner of the spokes used in this method, there will be leftover flaps that need to be dealt with, which are minimised by increasing the number of spokes. These portions result from discretising the developable cone inversion, and are shown in Fig. 2.6.

The second potential manufacturing method for performing the same fold is to use slider mechanisms for spokes, as shown in Fig. 2.5(b). In this method, the fabric is pushed down between the sliders in progressive steps, with each slider constraining it against the previous (more interior) one. The height of the packed pattern will be approximately equal to the height of the sliders. This pattern will have similar leftover flaps of fabric.

One way to account for the leftover flaps resulting from both methods is to wrap them in a clockwise or counterclockwise fashion around the compacted shape, similar to a collapsible umbrella. After the folding has taken place, the folding frame can be removed from the compacted fabric before packing the fabric into a cylindrical housing by wrapping the remaining flaps around the central portion and securing the fold with a restraint.

2.2.3 Deployment Rotation

When Soft Origami is used, rotation may occur during deployment. In the flasher and inverted-cone fold patterns, the main predictor of deployment rotation is whether flaps of material were wrapped in a circular pattern at any point in the packing process. In the case of the flasher pattern, as the pattern folds up, each portion of the soft-sheet-material experiences rotation due to the nature of the basic flasher pattern, which can be seen in three stages of deployment Figure 2.2. A packed Soft Origami flasher will rotate when deployed

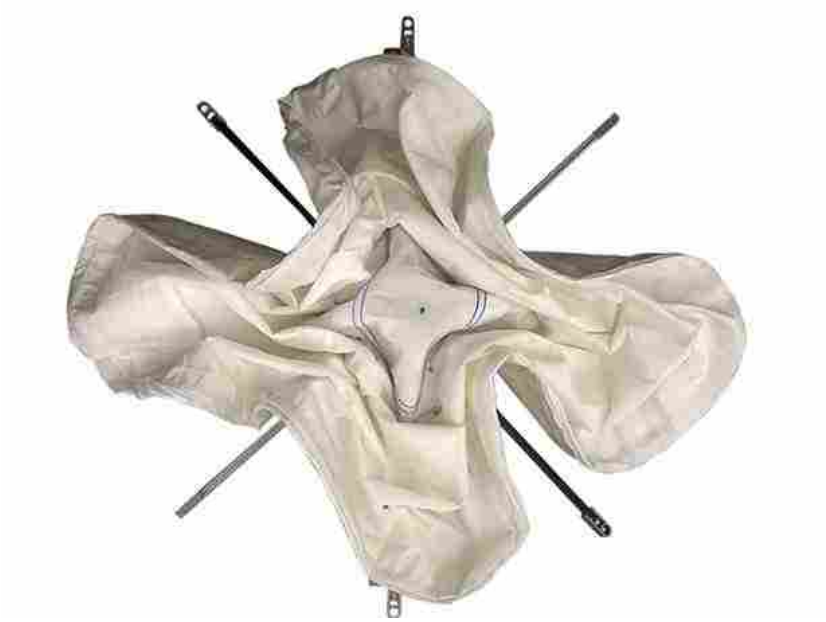

Figure 2.6: The inverted-cone fold shown in the middle of the folding process. Note the flaps of cloth that are unconstrained, which are then wrapped around the central portion to achieve the cylindrical packing.

as it travels through the reverse of its folding motion. Depending on how the inverted-cone fold was packed, there may or may not be rotation. If there are leftover flaps that must be wrapped around the central portion, as shown in Figure 2.6, there will be a corresponding rotation when deployed.

2.3 Application: Automotive Airbags

Driver's side airbags have previously been packed in rectangular prism shapes and the steering wheel shape designed to fit around the airbag unit. Recent trends point toward automakers using cylindrical steering columns and cylindrical central portions of steering wheels. As a result, current fold patterns have been modified to fit cylindrical mounts instead of rectangular mounts, which has resulted in less-than-ideal use of space due to gaps around the edges. Another approach that has been successfully used is a compression fold wherein the airbag is compressed into a cylindrical shape using a cylindrical mould and thousands of pounds of applied force. A base pattern that more closely approximates a cylinder is of

interest to improve packing efficiency. As such, airbags are a prime example of a soft-sheet material that needs to be folded into a cylinder and has critical deployment characteristics.

In collaboration with an automotive airbag manufacturer, Autoliv, the inverted-cone fold and flasher fold patterns were imposed on three driver's side airbag modules and deployed using standard test procedures. The original (baseline) fold pattern is shown in Fig. 2.7(b), where a rectangular prism fold pattern is packed into a cylindrical shape. Both cylindrical packing efficiency and deployment performance were tested to compare the different folds to the baseline. In this application, a comparison of "bag pack space used," or the height of space available for an inflator (the gas generating device, which typically is a metal cylinder) after the folded airbag was inserted into the airbag module, was also performed.

2.3.1 Packing Methods Applied

The aforementioned packing methods were applied to automotive driver's side airbags consisting of two circular soft-sheet-material disks sewn together around the outer edge and having an inflator inserted through a central hole in the bottom layer of material.

Flasher

The folding table method was applied to the airbag to pack the flasher pattern into a cylindrical shape. In this case, a folding table made from rigid matboard panels glued to a flexible substrate (to act as hinges along the fold lines) was created from calculated dimensions matching the desired stowed height and diameter. An airbag folded with the flasher pattern applied to it is shown in Fig. 2.7(a) with a comparison image of the baseline fold in Fig. 2.7(b). The flasher fold shows improvement in cylindrical packing efficiency. Considering how well the flasher fold stays within the boundary of the mount, compared to the baseline fold, there is a marked improvement. The bag pack spaces were not equivalent, with the flasher fold providing 2.5mm (10%) less bag pack space, shown in Table 2.1. Due to the bag pack space being worse, the flasher fold had mixed results in the requirement to fit into a cylindrical space efficiently in this particular application.

(a) (b) (c)

Figure 2.7: Top view of (a) flasher pattern imposed on an airbag in a housing, packed using a rigid folding table made of matboard and flexible hinge substrate for the flasher pattern, (b) baseline fold imposed on an airbag in a housing, folded using a traditional rectangular fold that has the corners compressed or forced inward in order to fit within the circular perimeter of the airbag housing, and (c) inverted-cone fold imposed on an airbag in a housing, packed using four slider mechanisms for the inverted-cone fold pattern. All patterns were compressed to the same height prior to images being taken. Note the black housing visible under (a) and (c) but not (b), preliminarily indicating more efficient cylindrical packing for the flasher and inverted-cone patterns.

Inverted-Cone Fold

The slider method was applied to the airbag to pack it into a cylindrical shape, with the resulting airbag shown in Fig. 2.7(c), alongside a comparison of the baseline fold in Fig. 2.7(b). For this prototype, the extra flaps left over when using a 4-spoke folding mechanism were wrapped in a clockwise direction around the rest of the airbag upon removal from the folding frame. Upon inspection, the inverted-cone fold shows improvement in the cylindrical packing efficiency. One comparison is to evaluate how well the inverted-cone fold stays within the boundary of the mount. In the case of the baseline fold, the outside edge of the mount

Table 2.1: Comparison of bag pack space (height) for baseline, inverted-cone fold, and flasher fold.

Fold Pattern	Bag Pack Space (height, mm)	% Less Than Baseline
Baseline	26	0
Inverted Cone Fold	25.8	0.8
Flasher Fold	23.5	10

is only visible in a few spots due to the folded airbag overhanging the outside edge of the shape. Furthermore, the packed height was approximately equal, with the inverted-cone fold providing only 0.2mm (0.8%) less bag pack space, shown in Table 2.1.

2.3.2 Deployment performance

The airbag modules were tested in airbag test facilities in collaboration with Autoliv. Figure 2.8 shows images taken of the deployments using high-speed video. Tests were run at ambient (room) temperature and followed common deployment test protocols. Desirable deployment characteristics were noted and observed in each test. Some of the more crucial characteristics, such as the central panel of the airbag presenting itself first to the occupant as well as minimal spin when deploying, were monitored closely. To compare rotation of the airbags, centrelines were added to each photo where the central panel is visible in order to make rotational comparisons more convenient.

Flasher

Comparing the flasher (F) performance to the baseline (B) in Fig. 2.8, at Time 1 (8ms) there is differing deployment status in B1 (baseline pattern) and F1 (flasher pattern). F1 is still in a cylindrical packed shape, and has begun to extend outward (toward the camera) but not radially.

Continuing the comparison at Time 2 (11.25ms), the majority of radial deployment has occurred in the Baseline pattern in B2, while the flasher folded airbag in F2 has not deployed far enough radially for the central panel to be clearly visible. F2 also shows undesirable rotation, binding, and whipping as it opens.

At Time 3 (22.25ms), B3 has completed its deployment and stabilised as desired. F3 is barely fully deployed and is twisted and off-centre. Following the frames shown here, F3 did not fully stabilise until after at least 30ms.

Analysis of the results by Autoliv personnel after multiple tests including the test shown in Fig. 2.8 concluded that the flasher pattern, while showing promising cylindrical packing efficiency, underwent approximately 180 degrees of rotation, which is undesirable

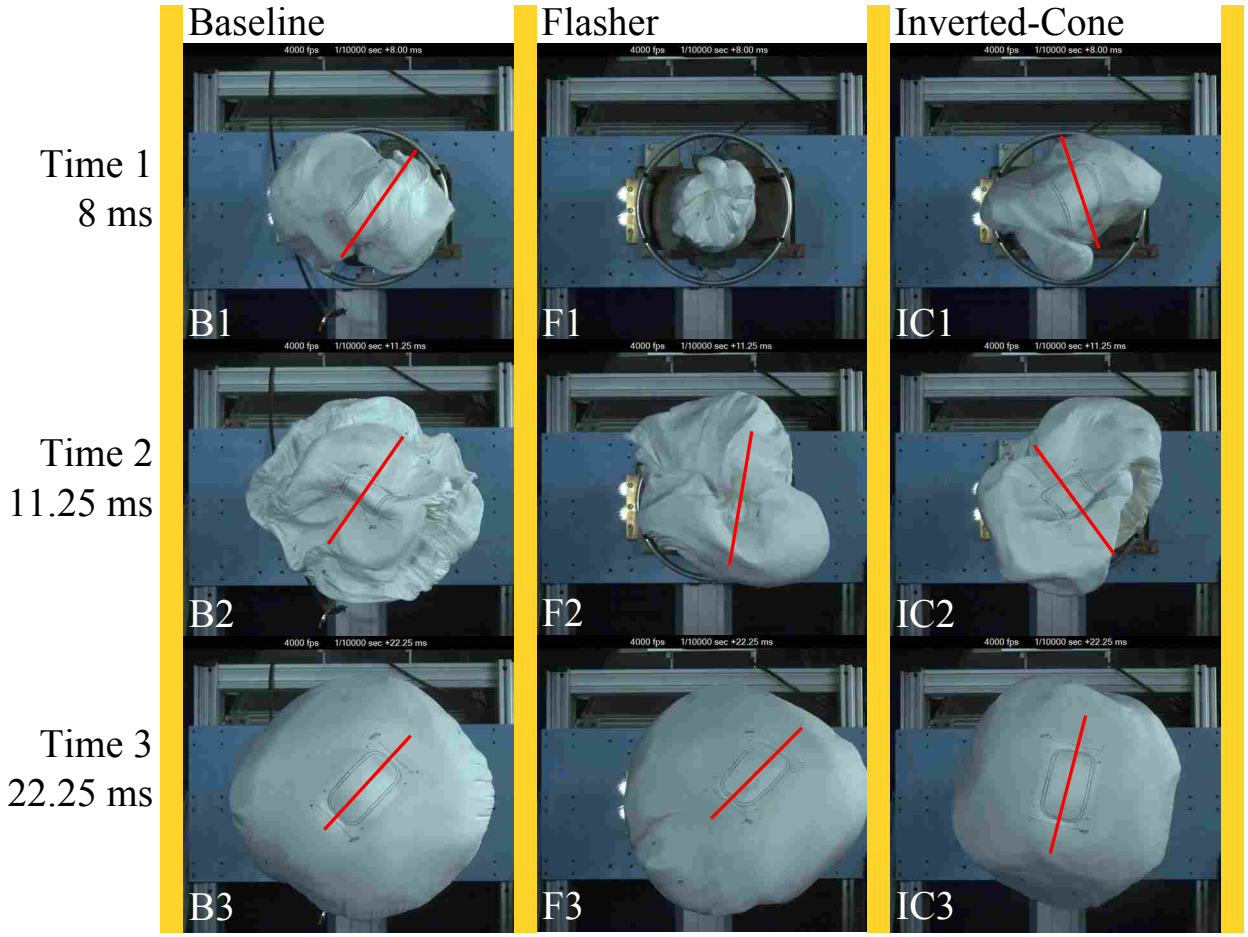

Figure 2.8: Images of three fold patterns implemented in airbags in live deployment tests. Patterns include the baseline fold, flasher fold, and the inverted-cone fold. Centrelines are imposed to show orientation of central panel. Columns represent different fold patterns, as labelled. Rows represent three different times: 1 - 8 ms; 2 - 11.25 ms; 3 - 22.25 ms. Images were taken at times when important deployment characteristics could be compared. All images were obtained in collaboration with Autoliv.

for the airbag application. It also did not deploy fast enough radially or present its central panel to the occupant as quickly as desired. For these reasons, additional work is necessary before it could be a viable fold option for application with a driver's side airbag. As a result of its poor performance in this application, the Flasher fold was removed from consideration as research moved forward.

Inverted-Cone Fold

Comparing the inverted-cone (IC) performance to the baseline (B) in Fig. 2.8, at Time 1 (8ms) we see similar deployment in B1 (baseline pattern) and IC1 (inverted-cone pattern). Both B1 and IC1 show favourable presentation of the central panel (blue rectangular outline in the centre) and similar, good deployment progression.

Continuing the comparison at Time 2 (11.25ms), we see that the majority of radial deployment has occurred in the Baseline pattern in B2, while the inverted-cone folded airbag in IC2 shows similarities but is slightly behind and is exhibiting less-than-ideal radial deployment. Specifically, B2 shows a more circular deployment while IC2 is deploying in a slightly oval shape.

At Time 3 (22.25ms), B3 has completed its deployment and stabilised as desired. IC3 is slightly behind in its deployment, and while it has deployed fully in the radial direction (it is presenting a fully circular front panel it can be seen that the central panel is rotated when compared to B3. This rotation shows that it is not completely stable. Following the frames shown here, IC3 did not fully stabilise until approximately 38ms, well after the acceptable time limit for stabilisation. Overall, it performed similarly to the Baseline pattern but showed some unfavorable rotation and stabilisation issues.

Analysis of the results by Autoliv personnel after multiple tests including the test shown in Fig. 2.8 concluded that the inverted-cone fold performed better than the flasher. It showed good radial deployment and promising deployment speed, and performed the closest to the baseline pattern. However, it did show an unwanted 90 degree twist which should be minimised before it can be implemented in commercial airbags. One cause of this twist is that the folding process results in multiple portions of the bag not packing into the original cylinder (flaps that extend out after the slider or slider link mechanisms are used to compress the material to the centre) and instead needed to be wrapped around the central shape to fit (thus leading to a spin when unwrapping). This is analogous to wrapping the remaining cloth around a collapsible umbrella when the arms are folded in and then using a strap to secure the wrapped cloth. Figure 2.6 shows an image of an airbag at this point in the folding process. Based on the promising performance and evaluation of the inverted-cone fold, research moving forward focused solely on improving the performance of this pattern.

2.3.3 Packing Method Modification Based On Deployment Performance

To address deployment performance, new packing methods were created for the inverted-cone fold to minimise rotational problems. The patterns remain the same, but new methods can be used to achieve performance closer to the desired function of this particular application. While the following methods can be used to improve the airbag deployment performance, other methods may be more appropriate for different applications. One of the main benefits of using Soft Origami is that the same base pattern can be used with different packing methods to achieve different deployment performance.

Two new packing methods were created to pack the inverted-cone pattern in a way that reduces rotational deployment spin. The first new packing method is called the Offset Cross Method, and it aims to increase the discretisation of the folds, that is, to increase the number of spokes (mentioned in Section 2.2 and shown in Fig. 2.4(b)). In this case, eight spokes were used to decrease the size of the flaps, thereby minimising the level of resulting deployment spin. The apparatus for this method consists of two cross mechanisms and two panels shown in Fig. 2.9(a)). In this method, the airbag is laid between the panels, and the first cross is inserted from the bottom into the bottom slots to generate the first fold. The cross is then actuated to compress the fold toward the centre. The second cross is then inserted from above into the opposite panel at a 45 degree offset, and actuated using the same process. The first cross is then removed, and the process is repeated until the airbag is completely folded. Figure 2.9(b) further depicts the offset nature of the panel slots, and the motion of the cross paddles.

This method was developed primarily for its ability to decrease flap size, but also because of its ability to be automated. Eight wide paddles (above and below) are re-used for each fold, which significantly decreases the number of degrees of freedom of the folding apparatus. The same airbag model used for to the baseline folded with the inverted-cone fold applied to it is shown in Fig. 2.10(a), alongside a comparison of the baseline fold in Fig. 2.10(b). For this prototype, the left over flaps on the right hand side were wrapped clockwise, while the flaps on the left were wrapped counter clockwise. The packing efficiency was similar to that of the baseline, but is expected to be improved with a well-developed folding apparatus.

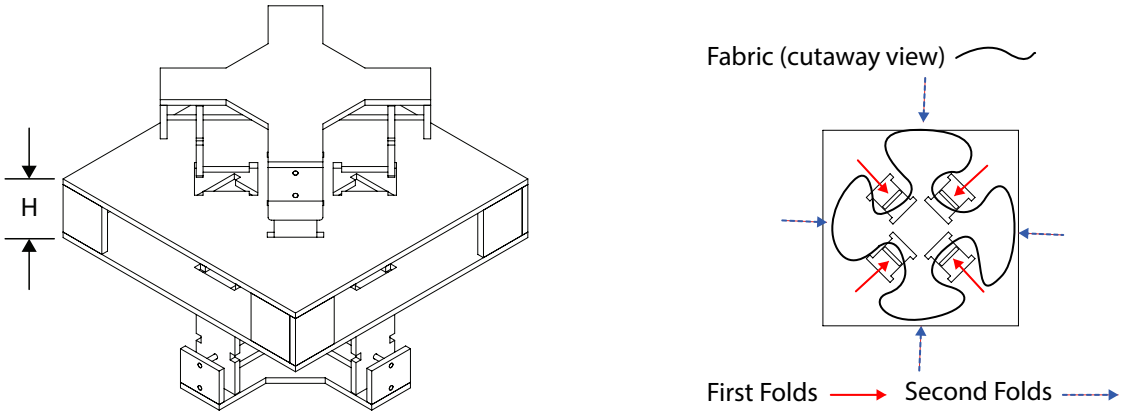

(a) (b)

Figure 2.9: Offset Cross Mechanism and fold sequence, with (a) isometric view of Offset Cross mechanism. Height H of the packed pattern can be selected by choosing desired offset between top and bottom panels. Note two sets of cross-shaped mechanisms, each with four slider mechanisms, with the top cross offset 45 degrees from the bottom, which are alternately inserted into the panels from the top and bottom and used to pack the inverted-cone fold pattern. In (b), we see a top view of a sample fold sequence, where the first set of folds are imposed in one direction and then the second set of folds are offset 45 degrees, thus increasing the discretisation of the fold and reducing the size of the leftover flaps.

The second new folding method is called the Nested Cylinder Method, and it aims to eliminate the extra flaps altogether by using continuous folds. The apparatus for the Nested Cylinder Folding Method consists of multiple cylinders, which are placed alternating from above and below (see Figure 2.11(a)). A cinching belt (made of a flexible sheet of polymer, textile, alloy, etc.) is also included. To fold, the material is placed over the first cylinder. A second cylinder with a larger diameter is brought down around the first cylinder, pushing a fold into the material. Successive cylinders are introduced in a like manner, from alternating directions, until the airbag is completely enclosed. The cinching belt is then placed around the outermost cylinder, and is tightened as each cylinder from large to small is removed. Figure 2.11(b) further depicts how the folds are created as cylinders are added.

This method is also easily automatable, and has the potential of using mechanisms with fewer degrees of freedom than the Offset Cross Method. A concern with this method is the friction between the cylinder edges and the fabric, but this can be mitigated with a refined surface finish and rollers placed around the edge of the cylinder. An airbag folded with the inverted-cone fold applied to it is shown in Fig. 2.10(c), alongside a comparison

(a) (b) (c)

Figure 2.10: Top view of (a) inverted-cone fold imposed on an airbag in a housing, packed using the described Offset Cross Method for the inverted-cone fold pattern, (b) baseline fold imposed on an airbag in a housing, folded using a traditional rectangular fold that has the corners compressed or forced inward in order to fit within the circular perimeter of the airbag housing, and c) inverted-cone fold imposed on an airbag in a housing, packed using the described Nested Cylinder Method for the inverted-cone fold pattern. All patterns were compressed to the same height prior to images being taken. Note the black housing visible under (a) and (c) but not (b), preliminarily indicating more efficient cylindrical packing for the inverted-cone fold offset cross and nested cylinder packing methods.

of the baseline fold in Fig. 2.10(b), showing similar improvement to previous patterns at packing into a cylindrical housing.

2.3.4 Deployment performance for new packing methods

Airbags were deployed at Brigham Young University to test the folding methods described above, with resulting images shown in Figure 2.12. Three flap treatments were also tested for the original slider mechanism: increasing from four to eight spokes (resulting in smaller flaps), clockwise and counter clockwise folded flaps, and map-folded (reversing pleats rather than being wrapped all in one direction) flaps. The deployments were filmed at a rate of 60 frames per second, on a test stand that uses compressed air to inflate the airbag (resulting in a deployment at about one-tenth of the speed of actual airbag inflators). Due to the difference in deployment method, further live deployment tests using standard test equipment and deployment speed would be necessary to directly compare these results with those obtained in collaboration with Autoliv and shown in Fig. 2.8. To determine whether

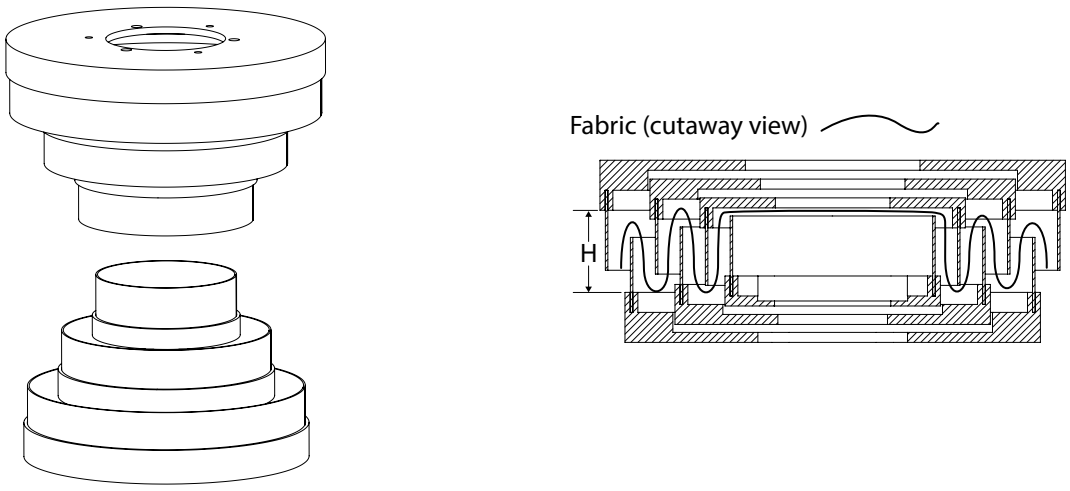

(a) (b)

Figure 2.11: Nested Cylinder Mechanism and fold sequence, with (a) isometric view of Nested Cylinder mechanism. Note multiple nested cylinders, which are inserted from alternate directions from small to large, imposing one layer of fold at a time. In (b), we see a cutaway view of the final fold configuration, with height H determined by height of interior cylinder, with the mountain and valley folds imposed on the airbag. A cinching belt is then placed about the outer cylinder, and is tightened as each successive cylinder is removed from large to small. This method evenly distributes all remaining flaps.

the inverted-cone fold performed similarly in both tests (and thus if the tests will likely show similar performance), an airbag folded using the same method and pattern was deployed and included in Fig. 2.12, labelled "Slider Mechanism," and it was seen in both cases that the angular rotation of the central panel between Time 1 and Time 3 was similar (albeit in the opposite direction, likely due to us wrapping the leftover flaps in the opposite direction), leading us to be confident that the compressed-air tests should show similar deployment characteristics. Each deployment was evaluated for rotational spin, and it was concluded that all of the different flap folding techniques, as well as the two airbag fold methods described previously (Offset Cross and Nested Cylinder), decreased deployment spin. To compare rotation of the airbags, centrelines were added to each photo where the central panel is visible in order to make rotational comparisons more convenient.

Examining the results presented in Figure 2.12, we see that at Time 1 the Slider Mechanism (S1) is still opening up and rotating clockwise, while the Folding Cross and

Nested Cylinder (FC1 and NC1, respectively) are more stable and further along through deployment. At Time 2, all three are nearly fully deployed radially, and we can see that the central panel (rectangle) of FC2 and NC2 are still aligned with their previous deployment photo and are more stable than S2. Finally, at Time 3 we see that all are fully deployed and stable. Both the Folding Cross Method and Nested Cylinder Method exhibit nearly zero rotation throughout deployment (as seen by the location of the central panel as well as the clarity of the photos indicating little movement), while the Slider Mechanism (the fold titled "inverted-cone fold" previously discussed in Section 2.3) exhibits a significant (greater than 30 degree) rotation.

2.4 Discussion And Conclusion

In this chapter, fold patterns and packing methods have been introduced and evaluated to efficiently pack soft-sheet materials into cylindrical packed shapes with configurable folded (packed) height and diameter, deployed (unfolded) shape, and deployed size. Deployment performance and the impact of packing method on deployment was also explored. Two fold patterns (the flasher and the inverted-cone fold) and a total of two packing methods for the first pattern and four for the second pattern were presented as viable solutions. Application to automotive airbags was explored and results showed promise, although the flasher was shown to be less-than-ideal for driver's side airbags and would likely be more valuable in other Soft Origami applications.

Both fold patterns have adjustable stowed height and diameter, deployed shape, and deployed size while folding into approximately cylindrical shapes. We were able to influence the behaviour of the airbag using this approach, and preliminary testing showed that we were able to specify packed behaviour, unfolding behaviour via pressure difference deployment, and final deployed shape. Both patterns showed favourable improvements in packing an airbag into a cylindrical shape with sufficient room underneath the packed material for an inflator.

Multiple possible methods were created and explored to fold the inverted-cone fold and flasher fold patterns using a rigid frame that is later removed. After frame removal, the folds are ready to be deployed by way of a pressure differential. The patterns, shown

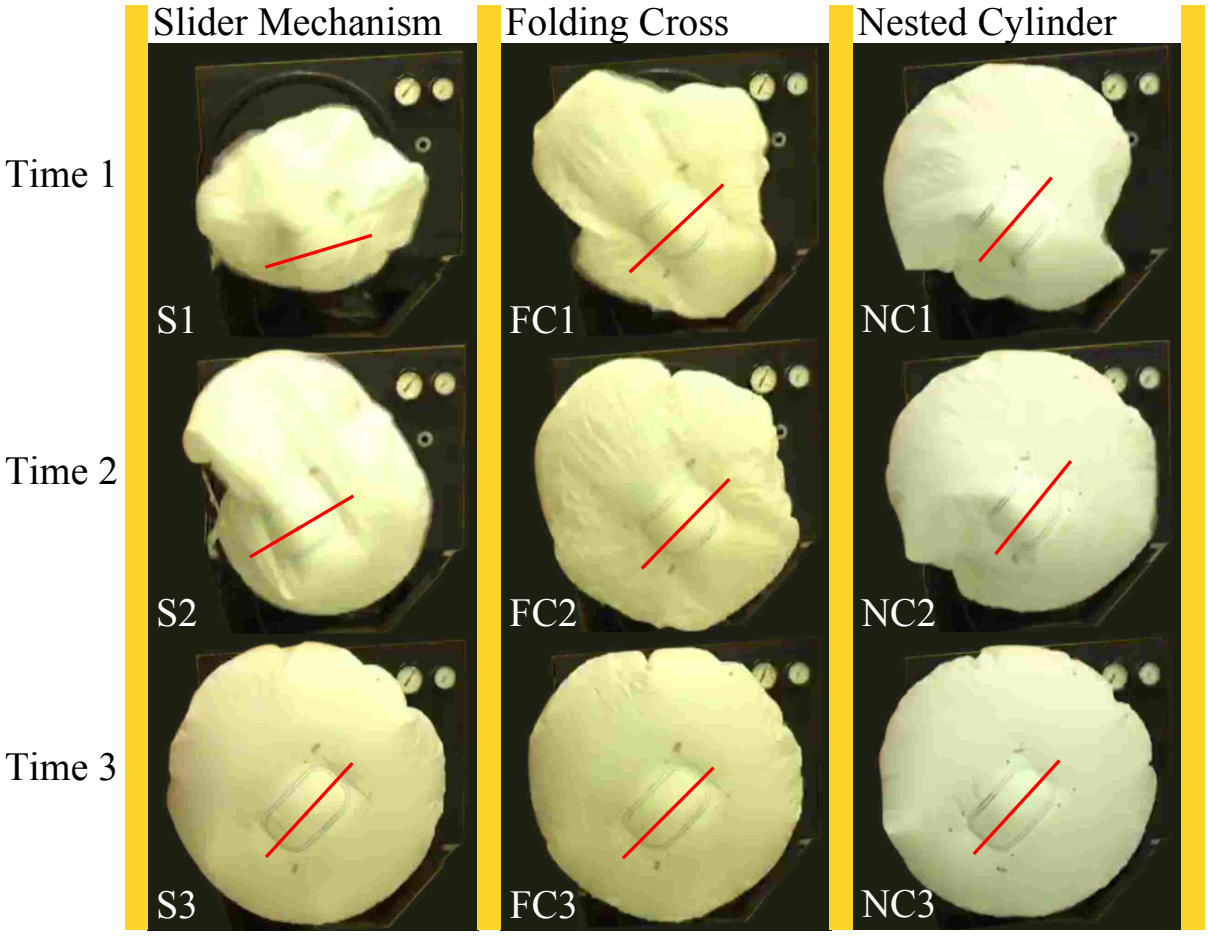

Figure 2.12: Images of three packing methods for the inverted-cone fold implemented in airbags in test stand deployment tests. Packing methods include the the slider mechanism (using 4 sliding mechanisms, the same method and pattern shown previously in Fig. 2.8 under the title "Inverted-Cone") as a baseline as well as the Folding Cross Method and Nested Cylinder Method. Centrelines are imposed to show orientation of central panel. Columns represent different packing methods, as labelled. Rows represent three different times. Images were taken at times when important deployment characteristics could be compared. The Folding Cross Method and Nested Cylinder Method appear to show less rotation upon deployment.

through an application to automotive airbag folding, accomplished the desired goals of the research. The packing methods demonstrated here have been shown to work when folded by hand (with a combination of a mechanism and human intervention), but have not yet been automated, which could be a topic of further work.

Another accomplishment of this research was the modification of packing method based on deployment performance. Although the same pattern (the inverted-cone fold) was

used, different packing methods were shown to influence deployment performance, which is likely true of many Soft Origami patterns and applications. That is, unlike traditional origami, where fold lines constrain behaviour, Soft Origami allows for a more quantitative approach wherein the same pattern can be packed using many different methods depending on the application constraints.

In conclusion, multiple patterns and packing methods were presented that are well-suited for packing a soft-sheet-material into a cylindrical volume prior to deployment via internal pressure. Another unique development in this work is the use of an origami-pattern-inspired folding frame to impose the pattern on the soft-sheet materials, and then removing the folding frame and maintaining the folded shape for use in deployment via pressure difference (e.g. inflation). This is advantageous for a mechanism or structure that would present a safety hazard to humans if it had a rigid understructure when deploying. In an application to automotive airbags, we also demonstrated the principle of modifying the packing method (within the same origami fold pattern) based on deployment performance and requirements.

CHAPTER 3. ARBITRARY PRISMATIC SHAPE PACKING

3.1 Introduction

The ability to pack folded materials into densely packed prismatic shapes is of interest in fields where flat sheet materials must be folded into a particular shape such as automobile airbags, camping equipment packing, map folding, possible reconfigurable packing material (to replace support material such as styrofoam in packages) and other soft-sheet applications. This chapter presents a preliminary study and method for packing sheet materials into prismatic shapes.

For the purpose of this research, a densely packed prismatic shape is defined as an arbitrary continuous shape (when looked at from the top or bottom) of constant height that does not have internal gaps. Classic examples include a rectangular or triangular prism, but a prismatic shape could be formed from an arbitrary closed curve as well. A polygonal prismatic shape is shown in Fig. 3.1, and prismatic shapes can also be shaped by continuous curves instead of polygons.

3.2 Background and Objective

This chapter evaluates the use of a special case of the Miura-ori pattern to pack sheet materials into prismatic shapes. The Miura-ori pattern is widely adaptable for different engineering applications. A sample Miura-ori pattern is shown in Fig. 3.3(a). Variations on the Miura-ori that have been created are the Miura, Tapered Miura, Arc, and Arc-Miura among others [7, 26, 27], and modifying some or all of the vertex fold angles can result in a wide range of behaviors. In the past, the Miura-ori has been found to be one ideal pattern for map folding. Unlike a typical map fold, the Miura-ori can create maps that have a single

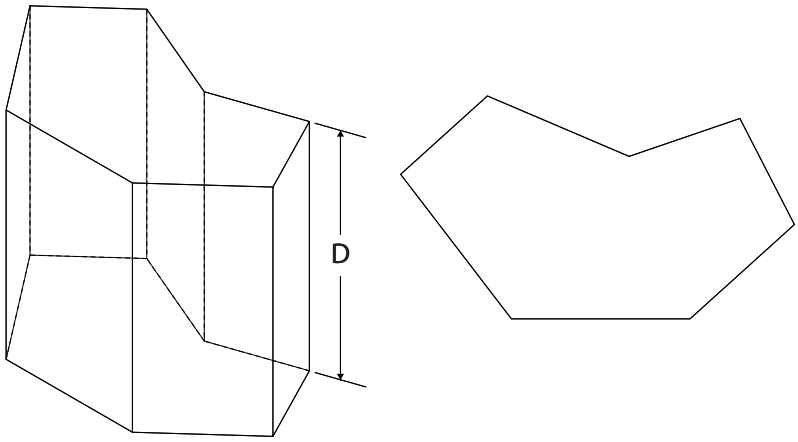

Figure 3.1: Angled view (left) with depth D shown and top view (right) of example Arbitrary polygon prismatic shape.

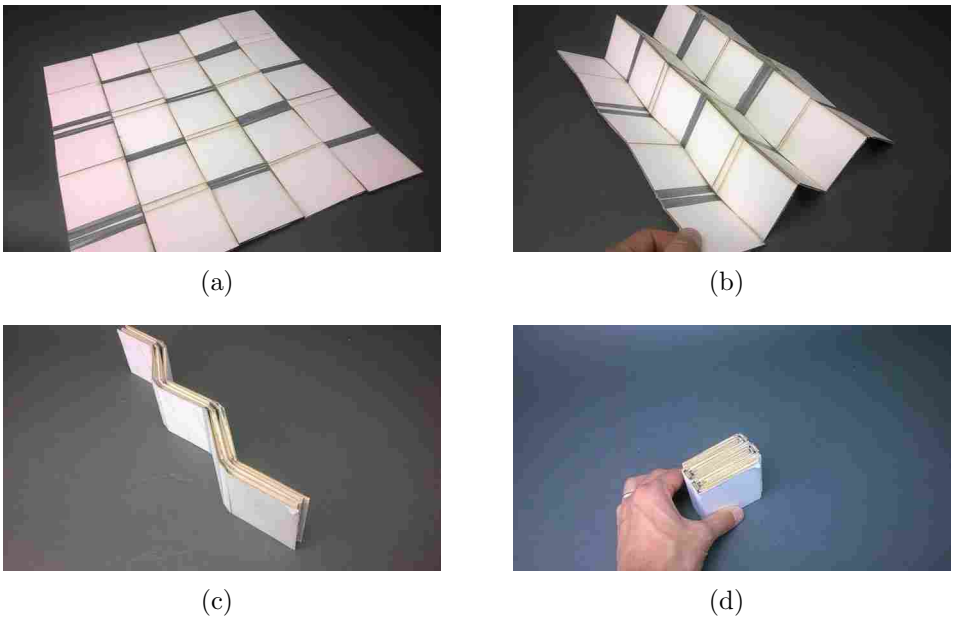

Figure 3.2: Fully-dense thick Miura map fold with (a) Flat, (b) Vertical mountain and valley folds partially actuated, (c) Vertical folds fully folded, and (d) fully-dense rectangular prism shape. Photos and prototype courtesy of Mary Wilson.

degree-of-freedom and are thus easier to open and less likely to rip when folded and unfolded repeatedly. A sample prototype of a thick-material Miura-ori map fold is shown in Fig. 3.2.

The objective of this preliminary study is to consider a method for folding a continuous flat sheet shape into a densely packed prismatic shape using a special case of the Miura-ori

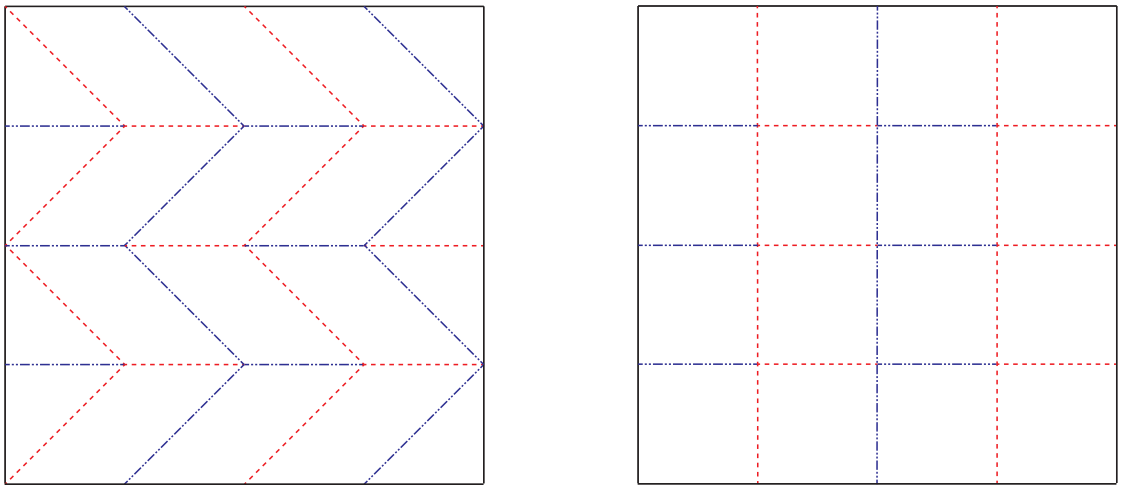

(a) (b)

Figure 3.3: (a) Regular Miura-ori, (b) 90 Degree Miura-ori.

pattern. This special case can be used to design a wide range of densely packed prismatic shapes. The original sheet material can also be a wide range of continuous flat shapes.

3.3 Ninety-degree Miura-ori

A typical Miura-ori crease pattern is shown in Fig. 3.3(a). Each vertex (point where fold lines intersect) in this pattern is a degree-four vertex; that is, there are four fold lines intersecting at each vertex. Vertex angles (angles between adjacent fold lines entering a common vertex) for the standard Miura-ori are between 0 degrees and 180 degrees, but are not all equal. For the case of the ninety-degree Miura-ori, all vertex angles are ninety-degrees. An example pattern of the ninety-degree Miura-ori is shown in Fig. 3.3(b). The ninety-degree Miura-ori could also be termed a simple grid pattern or be called a "doubly-pleated" fold. The pattern shown in Fig. 3.3(b) shows equally-spaced horizontal and vertical grid lines, but these lines do not need to be equally spaced for the pattern to fold. When the fold pattern with equal spacing is fully folded, it will approximately match a rectangular prism in overall shape.

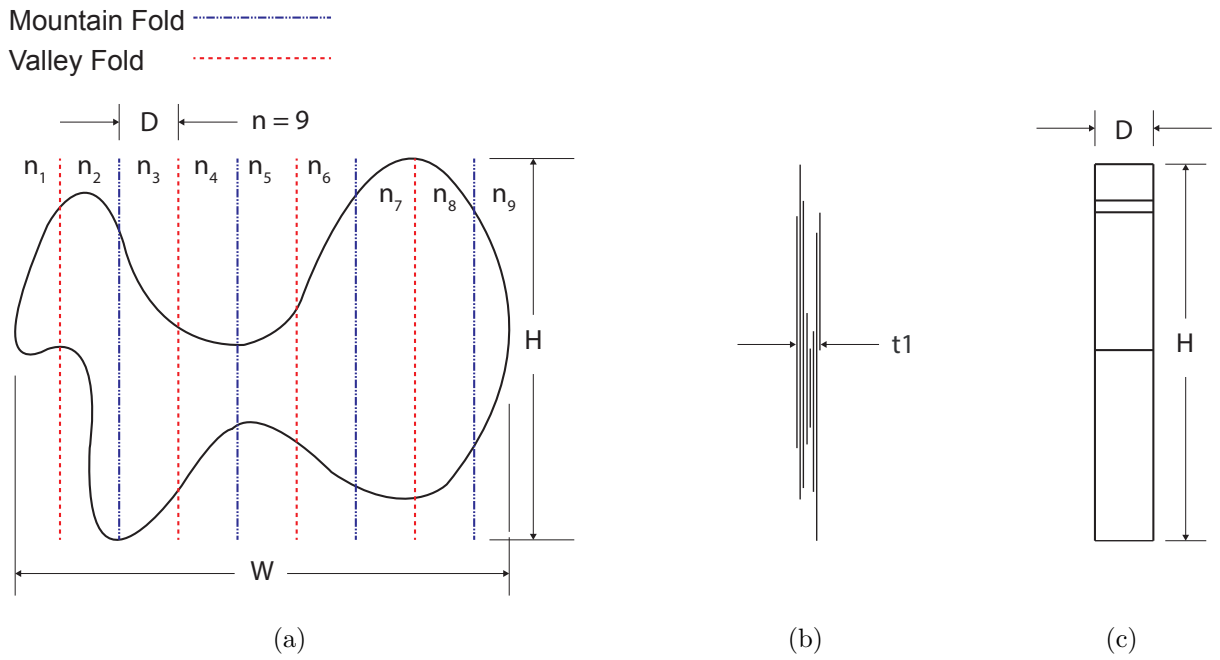

Figure 3.4: (a) Alternating vertical mountain and valley folds imposed on an arbitrary-shaped sheet material (solid line), (b) top view after folds are imposed, along with associated profile and overall shape thickness, and (c) side view of folded strip.

3.3.1 Application to arbitary-shaped flat sheet material

The ninety-degree Miura-ori can be applied to arbitrary-shaped flat sheets (not rectangular) if desired. As shown in Fig. 3.4, to fold an arbitrary-shaped flat sheet of material of overall maximum height H and width W using the ninety-degree Miura-ori pattern, a depth dimension D can be selected such that $D < W$. Alternate mountain and valley folds distance D apart, separating the sheet into n segments where $n = floor(W/d) + 1$, can then be folded. For a sheet of thickness t, when the mountain and valley folds are completed, the resulting pattern will form a folded strip of width t_1, where

$$t_1 = nt \tag{3.1}$$

Next a set of horizontal fold lines spaced arbitrary x_m distances apart can be imposed on the folded strip as shown in Fig. 3.5(a). For the case shown previously in Fig. 3.3(b), all x_m values are equal and as a result the final folded shape closely matches a rectangular prism. However, if the horizontal fold lines are spaced at irregular x_m distances, the final prismatic

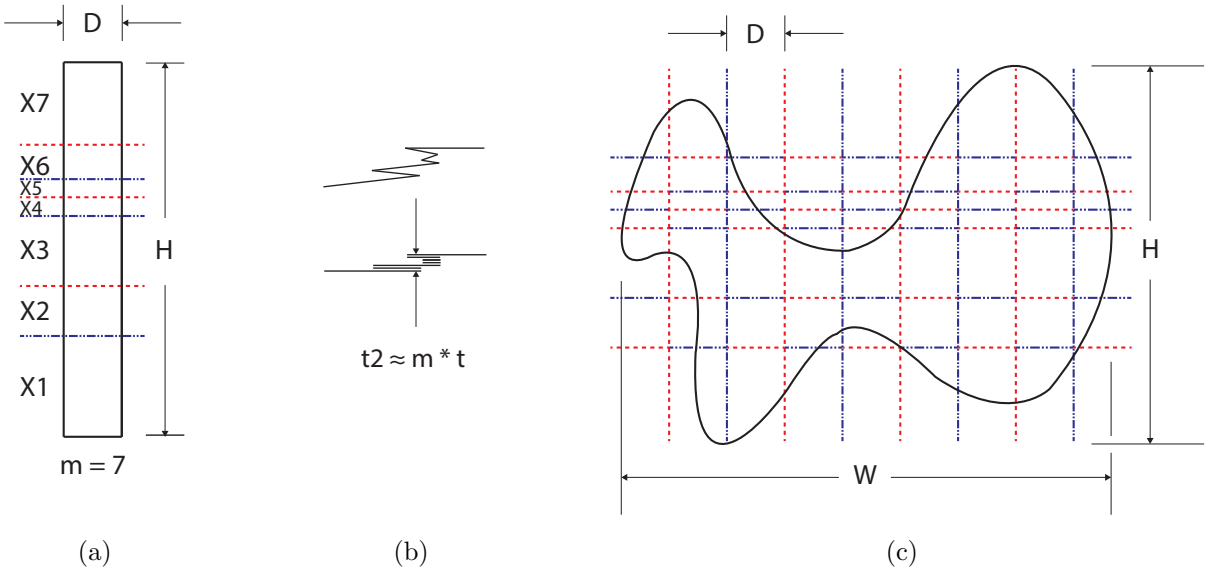

(a) (b) (c)

Figure 3.5: (a) Arbitrary-spaced horizontal grid imposed on folded strip from Fig. 3.4, (b) top view of strip folded at set lines with associated prismatic shape and overall width t_2, where m horizontal folds have been imposed, and (c) overall 90 degree Miura-ori fold pattern.

shape can be controlled to match a wide range of shapes in addition to a rectangular prism. This is shown along with a folded prismatic shape and the resulting overall fold pattern in Fig. 3.5(b) and Fig. 3.5(c). Note that if m is the number of horizontal folds imposed, the overall folded largest vertical dimension is

$$t_2 = mt_1 \tag{3.2}$$

These ideas can be applied to achieve a variety of folded prismatic shapes from arbitrary continuous flat sheets. It is also possible for a ninety-degree Miura-ori to double back on itself if necessary as shown in Fig. 3.7(c). A sample prismatic shape that could be matched is shown in Fig. 3.6(a). In Fig. 3.6(b) we see a way of representing the discretization of the shape. If the shape is approximated as a series of rectangles, with the width of each rectangle equal to t_1, the arbitrary shape can be matched by placing one fold inside each rectangle and alternating back and forth until the entire shape is filled.

As another demonstration of the possibilities of this method, the angle at which the folds start when matching an arbitrary shape can be varied to improve how well the

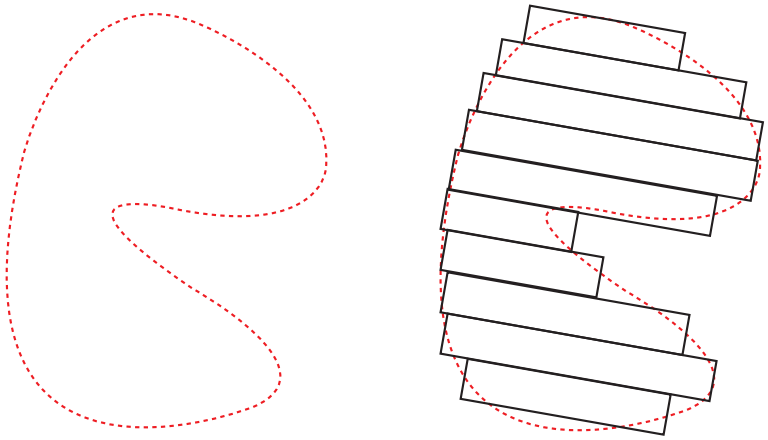

(a) (b)

Figure 3.6: (a) Prismatic shape (top view) formed by arbitrary closed curve outline (b) prismatic shape discretized with rectangles.

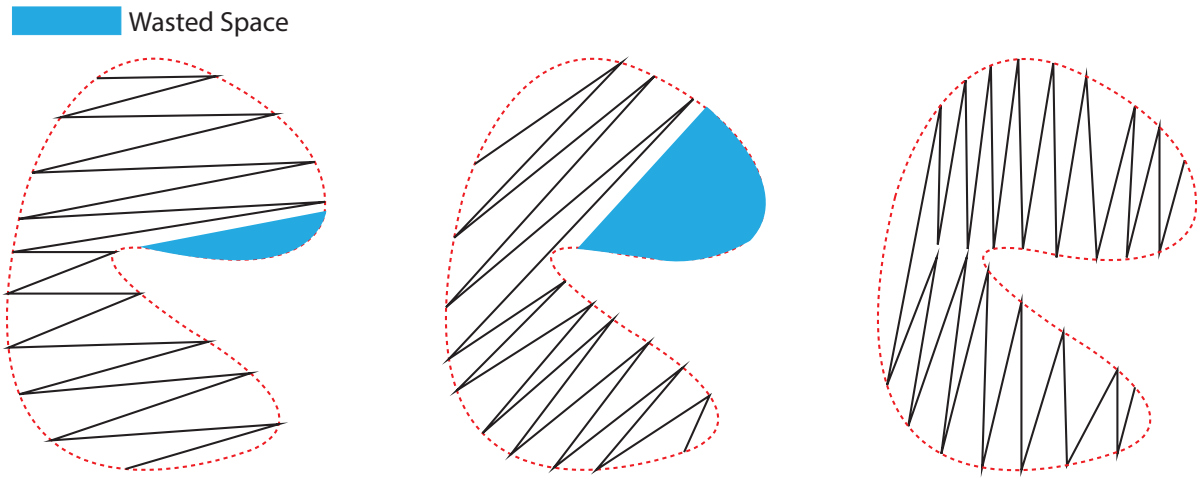

(a) (b) (c)

Figure 3.7: Examples with different fold configurations and starting angles and the resulting wasted space from each configuration.

pattern matches the arbitrary prismatic shape. In Fig. 3.7 we see three examples of the same prismatic shape with a ninety-degree Miura-ori fold filling the shape with material. In each case, we see a different angle at which the primary folds are placed, and we also see that some combinations result in less wasted space than others. Future research could study how to optimally fill such an arbitrary prismatic shape.

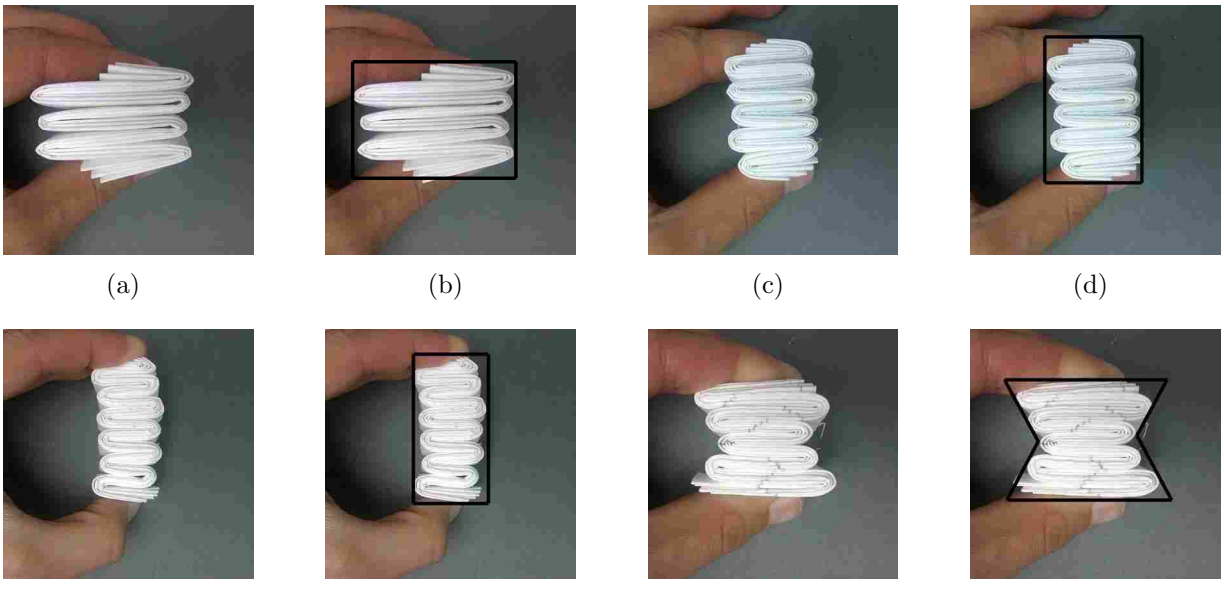

(a) (b) (c) (d)

(e) (f) (g) (h)

Figure 3.8: All patterns were made with a rectangular sheet of the same size. On the left of each pair (part (a), (c), (e), and (g)) we see the folded pattern and on the right (part (b), (d), (f), and (h) we see the prismatic shape. It should be noted that the prototype folded in (a) is the tallest (in the dimension coming out of the page), (g) is the second tallest, (c) is the third tallest, and (e) is the shortest due to starting with the same sized sheet.

Photographs of several arbitrary folded shapes folded from rectangular sheets of the same size sheet are shown in Fig. 3.8. Photographs of a circular flat sheet folded into an oval prismatic shape are shown in Fig. 3.9, and photographs and a flat pattern for an arbitrary shape with a preliminary offset pattern to account for thickness are shown in Fig. 3.10.

3.4 Discussion and conclusion

Thickness accommodation has not been discussed in this research. Should the number of vertical n and horizontal m folds be increased too much or the thickness t of the material be too high, there will be a functional limit on how many m times n folds can be folded back on themselves. One possible method to account for thickness, if the material is flexible and can stretch and/or wrinkle, is to offset or taper creases as discussed in prior research [4,28,29]. Further research would need to be done to determine how to account for conflicts at vertices if such a method is used on a non-flexible material. Further work could also be done to

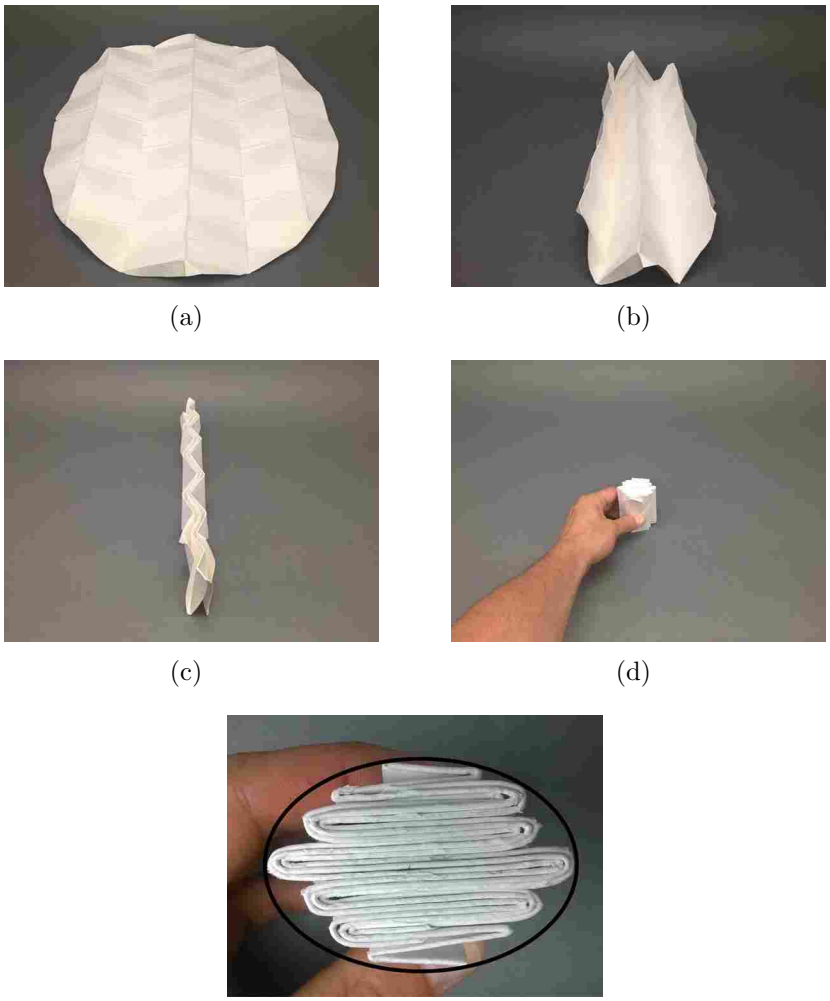

Figure 3.9: Progression of circular flat sheet folded into oval prismatic shape, with (a)-(d) showing fold progression and (e) showing prismatic shape from a top view.

examine the possibility of using reverse folds such as used in the Accordion pattern [30] to extend the densely packed shape into a 3D volume that is not necessarily prismatic. In conclusion, the objective of this preliminary study was met. A method was detailed using the ninety-degree Miura-ori to fold continuous flat sheet of arbitrary continuous shape into a densely packed prismatic shape. Using evenly spaced vertical fold lines and arbitrarily spaced horizontal grid lines was shown to be a viable method for designing a wide range of densely packed prisms. Thickness accommodation was addressed in brief, and further possible efforts were detailed.

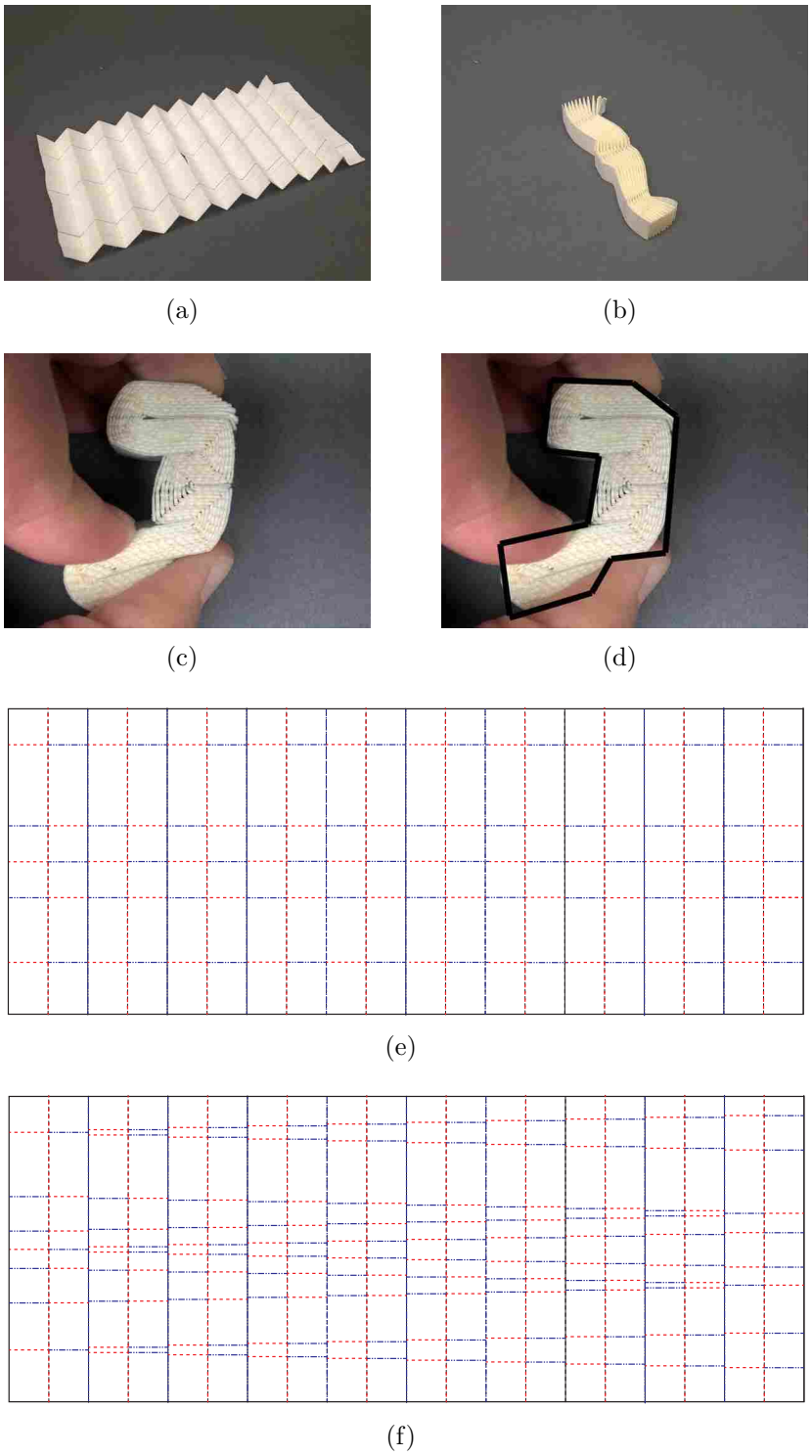

Figure 3.10: Progression of rectangular flat sheet folded into arbitrary prism pattern, with (a)-(c) showing fold progression, (d) showing prismatic shape from a top view, (e) showing original flat pattern, and (f) showing fold pattern as used in prototype modified to account for thickness by offsetting each progressive line (moving from n_1 to n_n) from the previous line by approximately the material thickness.

CHAPTER 4. SURFACE AREA EFFICIENCY FOR TRADITIONAL AND ORIGAMI-BASED CYLINDRICAL PACKING PATTERNS

4.1 Introduction and Background

Origami principles and engineering design have been explored in thick material applications, space applications, consumer products (such as clothing), and other fields [1, 2, 10]. One field that may benefit by being explored through the lens of origami is paper-based fluid filters. Filter material is similar to paper and starts as a flat sheet, so applying origami patterns and analysis methods to fluid filter design is a natural approach that allows for useful comparisons and analysis of the geometric efficiency of fluid filter designs, where geometric efficiency can be thought of as a measure of pattern surface area inside a given volume.

For the purpose of this research, "efficiency" is defined as the ratio of the surface area of a pattern compared to the surface area of a Idealized Model when packed into a cylinder of the same volume. There must be a minimum gap distance between filter elements to prevent "blinding," when one panel prevents another panel from being exposed to fluid flow.

In the case of rectangular filters, the current optimal design has converged on using alternating pleat folds arranged into a rectangular prism. While other patterns could be considered, the simplicity of an alternating pleat pattern and its ability to pack into a highly efficient pattern renders rectangular filter efficiency difficult to exceed.

However, cylindrical filter designs present an opportunity to apply new fold patterns to filters. Most current cylindrical filter patterns currently used have trade-offs in surface area and available dimensions, and have a large cylindrical hole in the interior [31, 32]. This type of cylinder geometric shape, with a cylindrical hole removed from the interior, will be referred to as an "annular cylinder" due to it being composed of an extruded annulus. A typical cylindrical fluid filter is shown in Fig. 4.1. Filters consisting of alternating mountain and valley folds wrapped around a cylinder like this have a larger hole in the center than

Figure 4.1: Typical cylindrical air filter with segment cut out to show interior.

would be necessary for the amount of fluid flow but because of a minimal gap distance requirement the inside diameter is constrained to always be greater than a certain value (depending on the required gap size). Patterns that do not require such a large central hole are of interest for optimizing efficiency with less of a trade-off in required dimensions.

Prior Origami and filter research has addressed patterns that fold into an annular cylinder. Some of these patterns include triangulated cylinders, a pattern titled the Kresling (which is a special case of a triangulated cylinder), expandable bellows patterns [33], rigid-foldable bellows patterns [34], cylindrical packing for expansion of solar arrays in space [4], and cylindrical origami patterns used for soft-flexible sheet materials such as airbags. As such, many equations and patterns are readily available for comparison to each other and a Idealized Model.

The objective of this research is to compare multiple patterns that are conducive to packing a large surface area into an annular cylinder through a structured analysis. Analysis is conducted from a purely geometric standpoint; that is, all analysis is based on geometric properties of the base fold patterns and is not combined with functional analysis specific to industries where these results could be applied. A Idealized Model is presented, and four patterns are considered: the Basic Pleat, M-pleat, Accordion, and Kresling. Two of the patterns are modified to provide a more consistent comparison; modifications are detailed below.

The approach that will be followed to achieve the research objective is to first define an idealized base model for comparison. Then, for each pattern, design parameters and

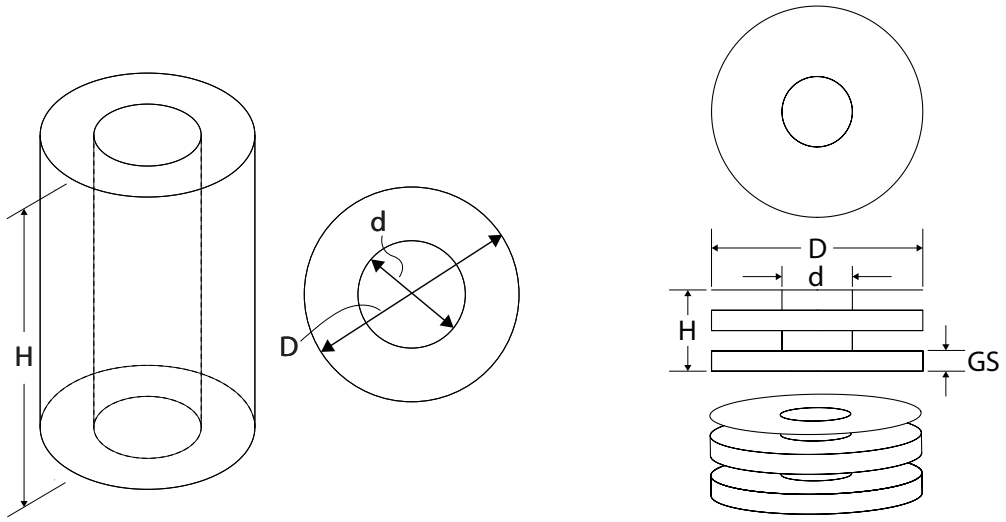

(a) (b)

Figure 4.2: (a) Defining variables of annular cylindrical volume and (b) idealized high-surface-area model, top, side, and angled views.

equations will be presented. Finally, efficiency analysis will be considered for each pattern before comparing all patterns at the same time. The annular cylindrical volume that each pattern will be designed to fit within (with defining variables height H, outer diameter D, inner diameter d), is shown in Fig. 4.2(a). These defining variables will be used throughout the chapter as each pattern is considered.

4.2 Idealized Model

The idealized high-surface-area model that fits within the outer cylindrical volume (created as a baseline comparison for all patterns) consists of a series of parallel annuli transverse to the longitudinal axis of the cylinder, each spaced an equal distance from the most prior annulus. Annuli are connected by cylindrical surfaces connecting the outside and inside edges respectively in an alternating fashion. Spacing between annuli ensures that, for applications such as fluid filters where such patterns could be used, there are spaces for flow to occur between panels, leading to a required gap size GS. Variables D, d, H, and new variable GS are detailed in Fig. 4.2(b). Because the origami models used in this study

assume material with zero thickness, the Idealized Model also assumes the panels have zero thickness.

The surface area of this model can be calculated by finding the number of annuli n that fit within a given height, using the floor function to insure an integer value, as

$$n = floor\left(\frac{H}{GS}\right) + 1 \tag{4.1}$$

The number of inner cylinders n_{inner} and the number of outer cylinders n_{outer} are calculated as

$$n_{inner} = \begin{cases} \frac{n-2}{2} & \text{if } n \text{ is even} \\ \frac{n-1}{2} & \text{if } n \text{ is odd} \end{cases} \tag{4.2}$$

$$n_{outer} = \begin{cases} \frac{n}{2} & \text{if } n \text{ is even} \\ \frac{n-1}{2} & \text{if } n \text{ is odd} \end{cases} \tag{4.3}$$

The number of annuli, inner cylinders, and outer cylinders are then multiplied by the respective area of each element. The disk model surface area, SA_i, is thus calculated as

$$SA_i = \frac{n\pi(D^2 - d^2)}{4} + n_{outer}\pi D \cdot GS + n_{inner}\pi d \cdot GS \tag{4.4}$$

Depending on the thickness of material t, number of layers, and gap size GS, the Idealized Model could be modified to account for thickness by substituting $GS + t$ for GS in the equation for n. The geometry models used for each pattern would then need to be examined on a case-by-case basis to identify necessary modifications to account for thickness t.

4.3 Basic Pleat design and comparison to Idealized Model

The Basic Pleat is one of the most common patterns currently used in fluid filters (commonly used in diesel and gasoline motors both to filter incoming air and circulating fluids). A physical example with a cut-away to see the interior can be seen in Fig. 4.1.

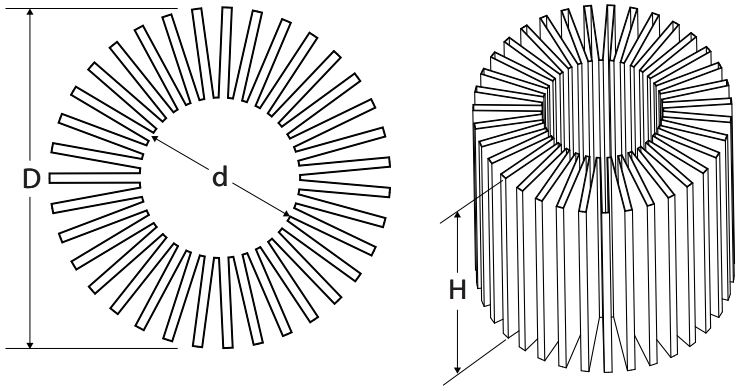

Figure 4.3: Top view (left) and angled view (right) of Basic Pleat pattern.

4.3.1 Basic Pleat design parameters

The geometry of the Basic Pleat consists of a set of alternating pleats imposed on a rectangular strip of material. Often, there are alternating sets of two mountain and then two valley folds, effectively creating a block "u" shaped pleat rather than a "v" shaped pleat. This is often done to maintain rigidity and spacing between folds. This Basic Pleat is then wrapped around a cylinder forming a hollow, annular cylindrical shape [35]. A top view and angled view of this pattern, with critical pattern dimensions D, d, and H are shown in Fig. 4.3. The base repeating unit in the fold pattern is composed of alternating long pleats with short double-line corner pleats between them which compose each of n_b pleats (with subscript b being used to distinguish that this is the number of pleats for the Basic Pleat) wrapped around the cylinder. A detailed view of several pleats and their associated flat pattern with dimensioned variables is shown in Fig. 4.4. In this figure as well as in other fold line diagrams shown in this chapter, mountain folds (coming out of the page like a mountain) and valley folds (going into the page like a valley) are shown using solid and dashed lines, respectively, to fully define how each pattern is folded.

Input values of D, d, H, desired minimum gap size IGS, and T_p (thickness of one pleat, or the width of one of the "u" shapes, assumed to be equal to IGS in this research) are used to generate the pattern. A constant gap size GS is used in each pattern to allow for direct comparisons in this analysis. The minimum value of IGS is $IGS_{min} = GS$ for this pattern, and for this research $T_p = GS$. More general equations are presented for cases

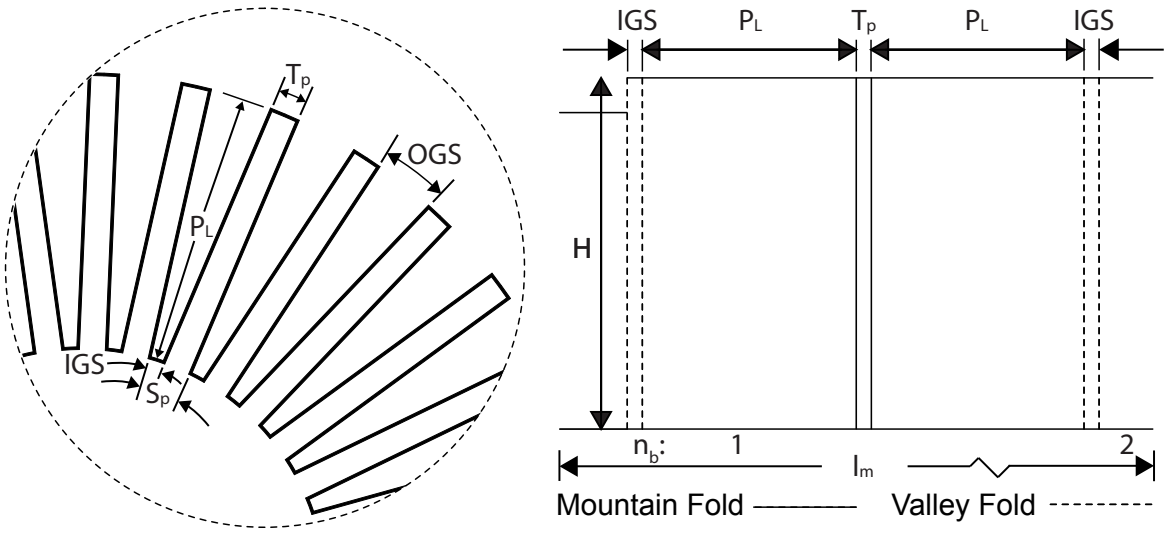

Figure 4.4: Detailed view of a portion of the Basic Pleat with variables used (left) and the base repeating unit flat pattern with dimensioned variables (right). Note that dashed lines are valley folds and solid lines are mountain folds on the fold pattern.

where $T_p \neq GS$. The equations used to fully define the pattern are given as follows: interior arc length S_p, total number of pleats n_b (rounded down using the floor function), and outer gap size OGS pleat length P_L, total pattern length l_b, and outer gap size OGS are defined as

$$S_p = T_p + IGS_{min} \tag{4.5}$$

$$n_b = floor\left(\frac{\pi d}{S_p}\right) \tag{4.6}$$

$$P_L = \frac{D-d}{2} \tag{4.7}$$

$$OGS = \frac{\pi D}{n_b} - T_p \tag{4.8}$$

Because we had to ensure integer values for n_b by rounding down, IGS and thus S_p must be adjusted to account for a resulting gap. This is done by determining the final interior gap size IGS and S_p as

$$IGS = \frac{\pi d}{n_b} - T_p \tag{4.9}$$

$$S_p = T_p + IGS \tag{4.10}$$

Finally, the overall length of the pattern l_b is

$$l_b = n_b(IGS + 2P_L + T_p) \tag{4.11}$$

$$\tag{4.12}$$

4.3.2 Basic Pleat efficiency analysis

These equations can be used to generate feasible Basic Pleat patterns. If d is decreased (so as to use more of the overall available cylinder), there will be a decrease in n_b and an overall decrease in pattern packing efficiency. Depending on the desired outcomes, the equations can be rearranged to calculate, for example, for a given a gap size and pleat width, what inner diameter d maximizes surface area for some given outer diameter D. Surface area SA_b of the pattern, to be used when comparing packing efficiencies, can be calculated as

$$SA_b = H \cdot l_b \tag{4.13}$$

These equations have been used to generate a range of patterns to compare to the Idealized Model. Figure 4.5(a) shows a plot comparing efficiency and D/d ratio for the Basic Pleat and Idealized Model with $T_p = GS$ and $GS/D = 0.015$. As expected, efficiency of the Idealized Model is equal to 1 across the range of D/d values. While peak efficiency is equal to 1 (the Basic Pleat and Idealized Model have equal surface area at $D/d = 1.0$), this result is of little practicality to the designer since at this D/d value both patterns are essentially hollow cylinders. As such, peak surface area is also of interest, and Fig. 4.5(b) shows the surface area values normalized by $H \cdot D$ used to generate the ratio shown in Fig. 4.5(a). The Basic Pleat achieves its highest normalized surface area value of 27.74 at $D/d = 1.9369$. Figure

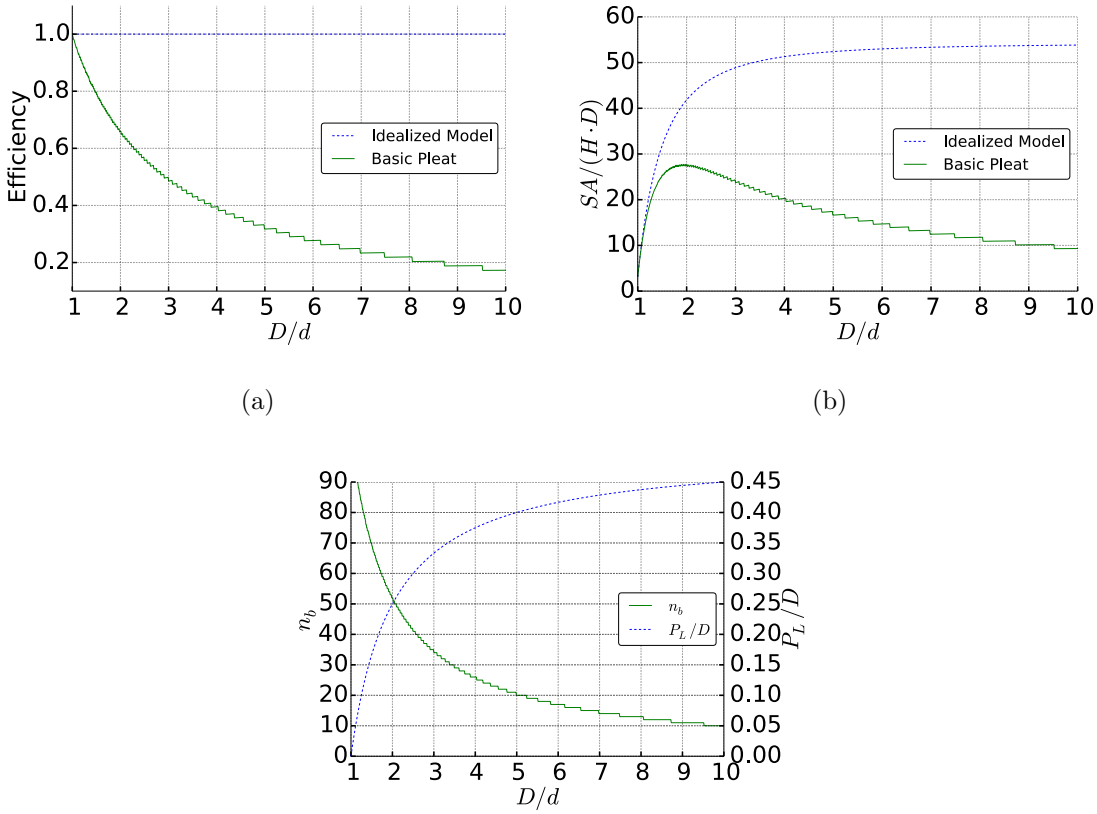

Figure 4.5: (a) Basic Pleat efficiency (SA_b/SA_i) and Idealized Model efficiency (b) Basic Pleat normalized surface area, with maximum value 27.74 occurring at $D/d = 1.9369$ (c) comparison of pleat length P_L/D and number of pleats n_b over range of D/d values for $D = 100mm$ and $GS/D = 0.015$ to explore sawtooth shape of other plots.

4.5(c) shows a plot comparing n_b and P_L normalized by D across the range of D/d values. Analyzing this plot, the discrete nature of the number of pleats, combined with a continual increase in P_L, is the cause of the sawtooth nature of the overall efficiency plot. As D/d increases and therefore d decreases, n_b decreases in a discrete manner, resulting in a sharp drop in overall efficiency followed by a gradual increase due to P_L continuously increasing before the next pleat is removed. However, if the maximum amount of material possible is desired and the inner diameter does not need matched exactly (as d decreases over the rest of the range), the peak values from $D/d = 1.9369$ could be used over the rest of the range and be valid.

Other GS/D values were considered at different D/d values to see if consistent results were achieved. A table considering peak efficiency values with GS/D ranging from 0.002 (observed in a commercial filter) to 0.03 is shown in Table 4.1. Examining this table, the value of GS/D at a specific D/d value has an impact in the peak efficiency, albeit small. A value of $GS/D = 0.015$ was chosen as a value in the middle of this range and used consistently for this research, although other values could be used.

Table 4.1: Basic Pleat efficiency values for a range of GS/D and D/d values.

GS/D	D/d					
	1.5	2	2.5	3	3.5	4
0.002	0.7983	0.6648	0.5706	0.4980	0.4432	0.3989
0.010	0.7911	0.6591	0.5614	0.4943	0.4339	0.3954
0.015	0.7879	0.6592	0.5572	0.4852	0.4292	0.3954
0.020	0.7881	0.6563	0.5591	0.4921	0.4321	0.3841
0.025	0.7768	0.6512	0.5622	0.4735	0.4175	0.3787
0.030	0.7803	0.6603	0.5460	0.4863	0.4165	0.3959

4.4 M-pleat design and comparison to idealized model

The geometry of the M-pleat (also called the "W-pleat") is similar to the Basic Pleat in that it is composed of alternating sets of two mountain and two valley folds imposed on a rectangular sheet of material. However, unlike the Basic Pleat, each successive pleat's length is not necessarily equal. Shorter pleats are added between some or all of the long pleats (thus resulting in an "M" shape when looking down on the folded pattern from above), reducing the wasted space resulting from the radial spread of each pleat in the Basic Pleat pattern. It has previously been found that the length of the shorter pleat should be close to half the length of the longer pleats to provide the best performance and stability [36]. Depending on the overall dimensions of the cylinder, they could, however, have different lengths and not be used between every normal pleat. Such irregular pleat length will not be considered in this work. Similar to the Basic Pleat, the M-pleat is also best executed with "u" shaped pleats rather than "v" shaped pleats.

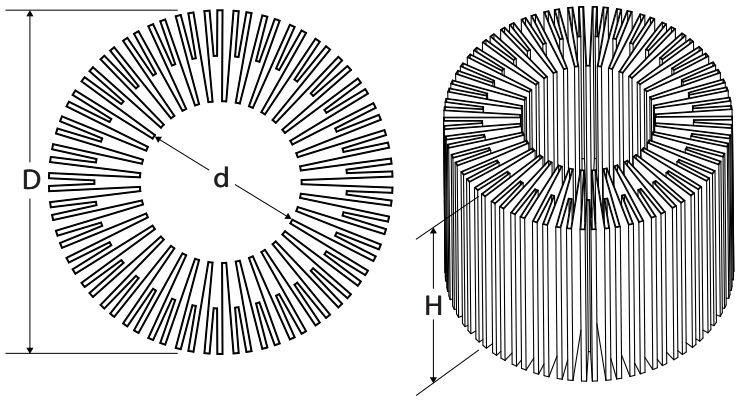

Figure 4.6: Top view (left) and angled view (right) of M-pleat pattern.

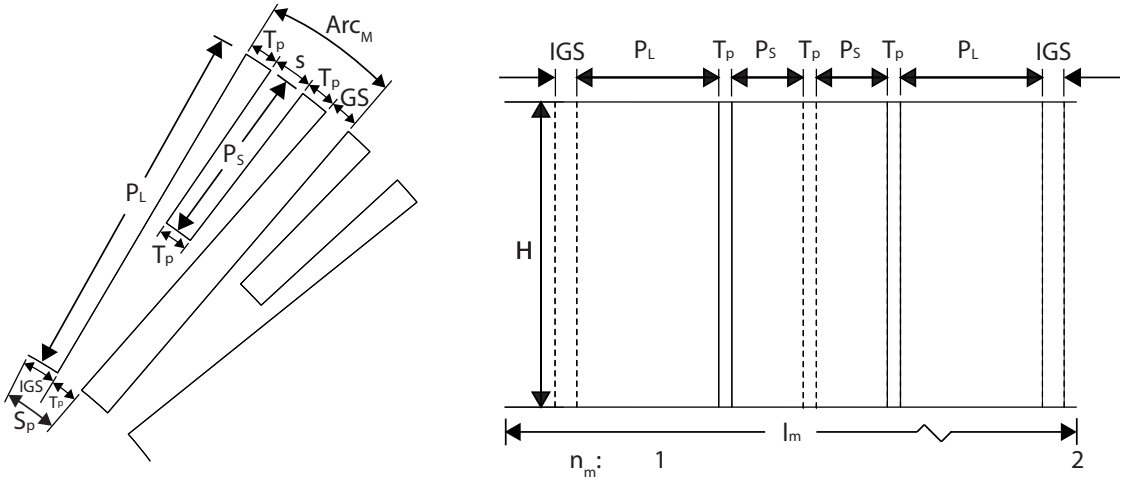

Figure 4.7: Detailed view of a portion of the M-pleat with variables used (left) and the base repeating unit flat pattern with dimensioned variables (right).

4.4.1 M-pleat design parameters

A top view and an angled view of this pattern, with D, d, and H are shown in Fig. 4.6. The base tesselation unit is composed of alternating long and short pleats, with small double-line corner pleats between them, with n_N normal long pleats and n_M modified M-pleats with an extra short pleat added between long pleats wrapped around the cylinder. A detailed view of several pleats and their associated flat pattern with dimensioned variables is shown in Fig. 4.7.

One form of the equations used to generate this pattern assumes input values of D (outer diameter), d (inner diameter), H (total height of cylinders), T_p (thickness of one

pleat, or the width of one of the "u" shapes), and a minimum gap size GS. Similar to the Basic Pleat, $T_p = GS$, and IGS is the inner gap size, although in the M-pleat this gap has a minimum value but must be calculated. Long pleat length P_L is calculated in the same manner as for the Basic Pleat as

$$P_L = \frac{D - d}{2} \tag{4.14}$$

While short pleat length P_S could be varied, based on findings of prior research [36] it is set equal to

$$P_S = 0.5P_L \tag{4.15}$$

Similar arcs can be used to find s and external arc length Arc_M required per M-pleat as

$$s = \frac{T_p\left(P_L + \frac{d}{2}\right)}{\frac{d}{2} + P_L - P_S} \tag{4.16}$$

$$Arc_M = 2T_P + GS + s \tag{4.17}$$

Now, the minimum value for IGS assuming the outside gap GS is maintained is

$$IGS = IGS_{min} = \frac{d(2T_P + GS + s)}{D} - T_P \text{ where } IGS_{min} \geq GS \tag{4.18}$$

Total inside arc length S_p is therefore defined as

$$S_p = IGS + Tp \tag{4.19}$$

Total number of pleats n_M is, using the floor function to insure integer values,

$$n_M = floor\left(\frac{\pi d}{S_p}\right) \tag{4.20}$$

Because we had to ensure integer values for n_M by rounding down, there will be a small gap using the current IGS calculation. The new IGS will be slightly longer than IGS_{min}, and is

$$IGS = \frac{\pi d}{n_M} - T_p \tag{4.21}$$

Using these values, total pleat length l_m is calculated as

$$l_m = n_M(IGS + 2P_L + 3T_p + 2P_s) \tag{4.22}$$

4.4.2 M-pleat efficiency analysis

These equations can be used to generate feasible pleat patterns. Depending on the desired outcomes, these equations can be rearranged to calculate various parameters. Surface area SA_m of the pattern, to be used when comparing packing efficiencies, can be calculated as

$$SA_m = H \cdot l_M \tag{4.23}$$

Figure 4.8(a) is a plot comparing efficiency for the M-pleat and Idealized Model for a range of D/d values with $T_p = IGS = GS$ and $GS/D = 0.015$. As expected, efficiency of the Idealized Model is equal to 1 across the range of D/d values. While peak efficiency is equal to 1 (the M-pleat and Idealized Model have equal surface area at $D/d = 1$), the M-pleat also essentially forms a hollow cylinder and is of little use to a designer. Surface area normalized by $H \cdot D$ is shown in Fig. 4.8(b). Examining this plot, we see a peak normalized surface area of 41.64 at $D/d = 2.2252$. Like the Basic Pleat, we see sawtooth behavior, and Fig. 4.8(c) compares n_m and P_L and P_S normalized by D across the range of D/d values. Again, the discrete number of pleats is what leads to the sawtooth nature when combined with the continual increase of P_L and P_S. There is a wide range in the beginning where the number of pleats is decreasing infrequently which leads to the first two steps being much longer than those after the peak. Again like the Basic Pleat, if the designer is seeking the maximum amount of material and is not concerned about matching the inner diameter exactly (as d decreases over the rest of the range), the peak value from $D/d = 2.2252$ could be used over the rest of the range and be valid.

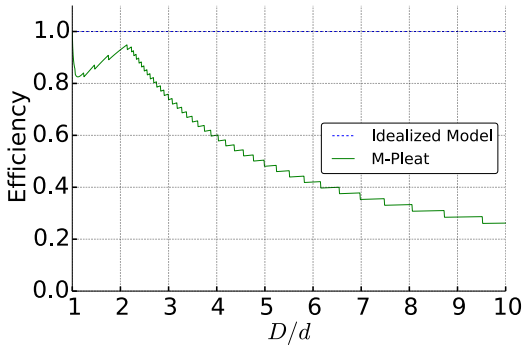

(a)

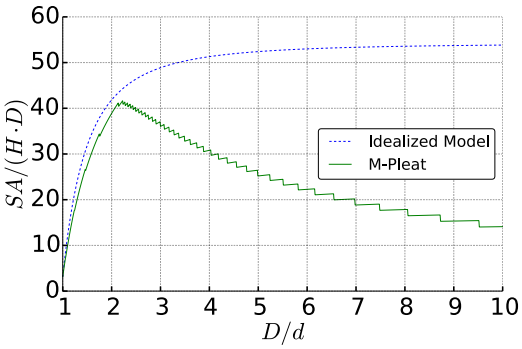

(b)

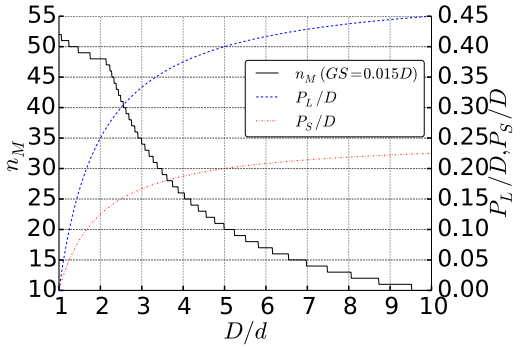

(c)

Figure 4.8: (a) M-pleat efficiency (SA_m/SA_i) and Idealized Model efficiency (b) M-pleat normalized surface area, with maximum value 41.64 occurring at $D/d = 2.2252$ (c) comparison of pleat lengths P_L/D, P_S/D and number of pleats n_M over range of D/d values for $D = 100mm$ and $GS/D = 0.015$ to explore sawtooth shape of other plots.

Other GS/D values were considered at different D/d values to see if consistent results were achieved. A table considering peak efficiency values with GS/D ranging from 0.002 (observed in a commercial filter) to 0.03 is shown in Table 4.2. Examining this table, the value of GS/D at a specific D/d value has an impact in the peak efficiency, more so than in the Basic Pleat, which could be due to the longer length per pleat of the M-pleat and the number of pleats being a discrete value.

Table 4.2: M-pleat efficiency values for a range of GS/D and D/d values.

GS/D	D/d					
	1.5	2	2.5	3	3.5	4
0.002	0.8574	0.9233	0.8577	0.7485	0.6661	0.5994
0.010	0.8599	0.9240	0.8508	0.7484	0.6563	0.5981
0.015	0.8615	0.9296	0.8482	0.7374	0.6517	0.6006
0.020	0.8705	0.9307	0.8554	0.7518	0.6589	0.5848
0.025	0.8576	0.9080	0.8645	0.7244	0.6376	0.5781
0.030	0.8647	0.9463	0.8403	0.7478	0.6376	0.6082

4.5 Accordion design and comparison to Idealized Model

The Accordion pattern is the first of two Origami-based cylindrical packing patterns. The underlying pattern has been studied from an origami perspective as a pattern useful for expanding and contracting in a longitudinal direction [30]. One essential difference between this pattern and the traditional patterns discussed prior is the propensity of the Accordion surfaces to lie in a nearly-horizontal plane if the pattern is placed on its end. The two traditional patterns discussed previously both have surfaces in the vertical direction. Having surfaces primarily in the horizontal direction requires a different approach to design because to add more material the pattern must be made taller and not wider.

4.5.1 Accordion design parameters

The geometry of the Accordion pattern consists of a set of repeated base polygons arranged in an alternating pattern and stacked in stories. A base tesselation unit polygon and its required variables a, b, c, and ϕ is shown in Fig. 4.9(a), with a wireframe view of a folded unit shown in Fig. 4.9(b) for reference. Inputs for the equations used to define the base unit include the interior diameter d and exterior diameter D of the annulus the pattern lies inside as well as n, the number of sides of the polygon forming the bottom of the folded Accordion. This pattern and others similar to it have been previously applied to filter design [37–40]. One form of the equations used to define the Accordion base unit is as follows [30], with the base unit shown in Fig. 4.9(a).

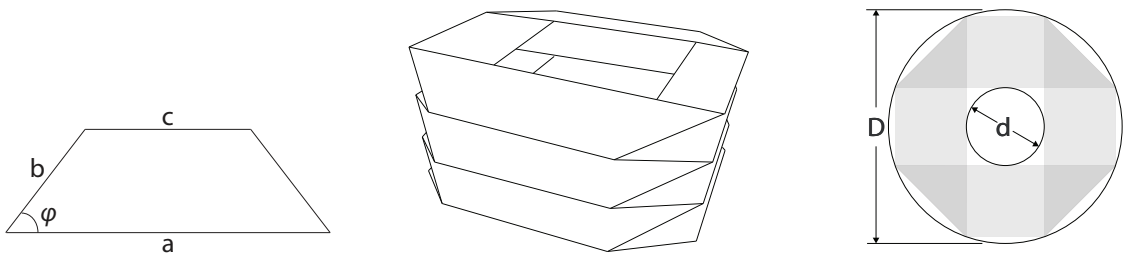

(a) (b) (c)

Figure 4.9: (a) Accordion base tesselation (b) angled view of folded Accordion with four sides and (c) top view with outer diameter D of circumscribed outer circle and inner diameter d of inscribed inner diameter shown.

$$\phi = \frac{\pi}{n} \tag{4.24}$$

$$a = \sqrt{D^2 - d^2} \tag{4.25}$$

$$b = D \sin\left(\arcsin\left(\frac{a}{D}\right) - \phi\right) \tag{4.26}$$

$$c = a - 2b\cos\left(\phi\right) \tag{4.27}$$

The Accordion pattern has n_a fundamental alternating units on each story. That is, an Accordion with $n_a = 4$ would have four repeating units on each story that wrap around to form the pattern when folded. For a valid fold pattern n_a must be an even number and $n_a \geq 4$. As n_a is increased, the pattern will more closely match a circular annulus but have increasing manufacturing complexity, and there are functional limits on the annular shapes that can be matched depending on the ratio of D/d. The parameter n_a can be chosen arbitrarily or allowed to change as part of an optimization routine, depending again on the ratio of D/d.

The final parameter used to fully define the flat pattern is s_a, where s_a is the number of stories. A pattern of base tesselation units with $n_a = 4$ and $s_a = 4$ is shown in Fig. 4.17. Because each story connects with each adjacent story with a sharp, angular crease rather than a squared-off double pleat (the "u" shape shown in the Basic Pleat and M-pleat),

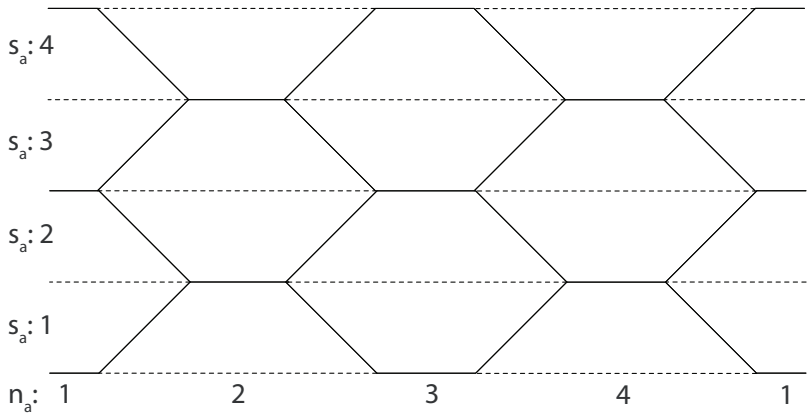

Figure 4.10: Accordion flat pattern with $s_a = 4$ and $n_a = 4$. Mountain folds are solid lines and valley folds are dashed lines.

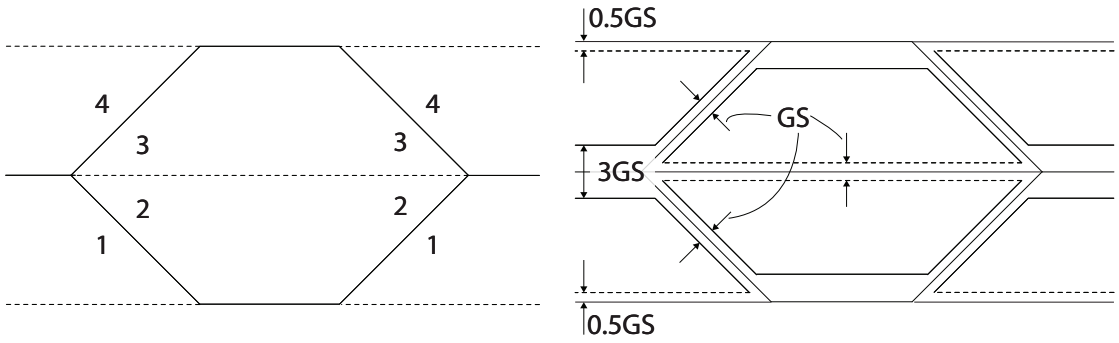

(a) (b)

Figure 4.11: (a) Layer ordering of two adjacent Accordion vertices and (b) offset line pattern using offset crease method. This portion of the Accordion pattern is a smaller portion of the diagram presented in Fig. 4.10 and these offsets are applied to the entire pattern before folding.

the pattern must be modified to accurately determine s_a and provide a more consistent comparison to the other fold patterns and the Idealized Model.

4.5.2 Accordion pattern modification

The Accordion pattern can be modified using an offset crease method [41]. For this pattern, layer ordering can be used to determine appropriate offsets for each crease. In prior applications of the offset crease method with thick materials, material is removed at the vertices to prevent self-intersections. In this application, the ability of the filter or paper

material to wrinkle and create "soft-creases" in the vertex areas and along creases eliminates the need to remove material. For the application of filters, this characteristic is essential for any pattern used in order to maintain continuous filter material without any perforations or holes. However, it also introduces uncertainty as the behavior of the material at the vertex cannot be reliably predicted.

As shown in Fig. 4.11(a), layers can be ordered from 1 to 4 in their sequential stacking order (when the pattern is fully folded, 4 lies directly on top of 3 which is directly on top of 2 which is directly on top of 1). Offsets for each crease between layers are then determined by finding the difference in panel number around shared creases and multiplying a unit desired gap by the resulting number to find the total gap size required about that crease. Thus, if the desired gap is the Gap Size GS, the total offset between panels 1 and 2 is $GS(2-1) = GS$. Likewise, the total offset between panels 2 and 3 as well as 3 and 4 is GS. When comparing panels 4 and 1, however, the offset will be $GS(4-1) = 3GS$. Once offsets are determined, crease lines can be offset half of the required gap on each side and trimmed to make continuous polygons. The pattern with calculated gap sizes is shown in Fig. 4.11(b). It should be noted that as shown in Fig. 4.11, when multiple adjacent vertices are considered, shared panels have the same calculated offset on both vertices.

Performing the offset crease method ensures that each panel is parallel and horizontal in its folded state, and allows for direct comparison with the U shaped folds of the Basic Pleat and M-pleat. A physical prototype was created, shown in Fig. 4.12 with achieved offsets between panels. It should be noted that if the value of GS is too large, the overall diameter D of the actual prototype will be smaller than the desired D value. It is assumed that applications such as filters that might use this research will have a GS small enough ($GS/D \leq 0.03$) to not present a major problem in this regard.

Because each vertex is an intersection of two stories, and because there will be an offset and gap of $\frac{1}{2}GS$ on either the top or bottom of each story, the total gap size required for each set of two layers is $4GS$. Therefore, the total number of required stories s_a for the overall height H is equal to H divided by one half of the overall $4GS$ spacing.

$$s_a = floor\left(\frac{H}{2GS}\right) \tag{4.28}$$

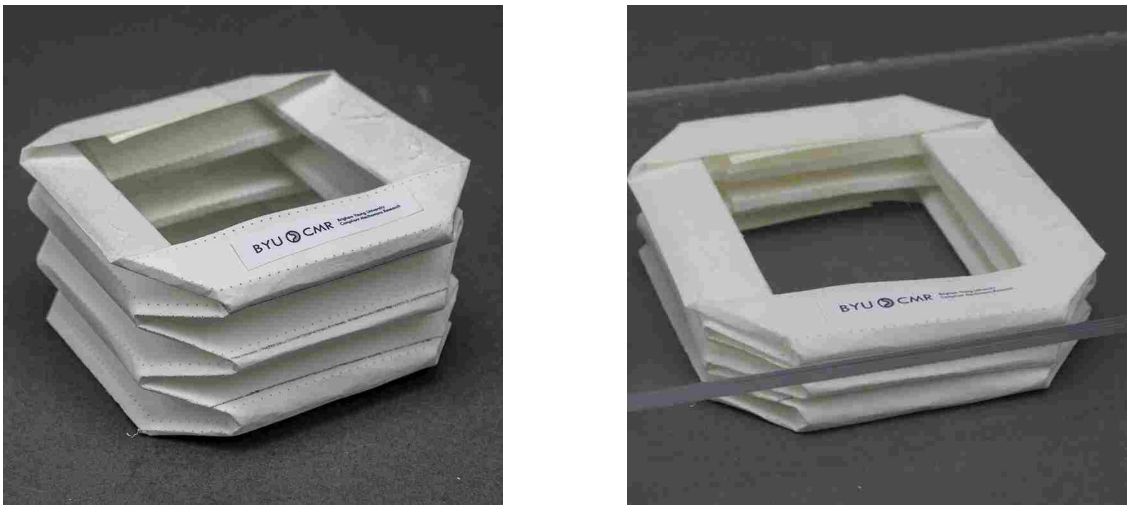

(a) (b)

Figure 4.12: Accordion prototype with $n_a = 4$ (a) uncompressed and (b) compressed.

4.5.3 Accordion efficiency analysis

Using these equations, a wide range of Accordion patterns can be designed. Given a specified inner diameter d, outer diameter D, number of sides n_a, overall height H, and minimum gap size GS, the pattern can be fully generated. Surface area SA_a can then be calculated as the surface area of the flat pattern, and is

$$SA_a = n_a \cdot s_a \cdot b \sin(\phi) \left(\frac{a+c}{2} \right) \tag{4.29}$$

These equations were used to generate patterns to compare to the Idealized Model. One primary characteristic that is of interest is the effect of n_a on overall efficiency. A plot comparing efficiency for a range of n_a values and across a range of D/d values, as well as the efficiency of the Idealized Model, is shown in Fig. 4.13(a). As expected, the efficiency of the Idealized Model is equal to 1 across the range of D/d values. Surface area normalized by $H \cdot D$ is shown in Fig. 4.13(b). In order to more closely examine the results, another set of efficiency and surface area plots are shown in Fig. 4.13(c) and Fig. 4.13(d) respectively, with D/d ranging from 1.0 to 4.0.

Maximum efficiency values, associated D/d values, and maximum normalized surface area (which occurs at the same D/d values as maximum efficiency and continues on for the

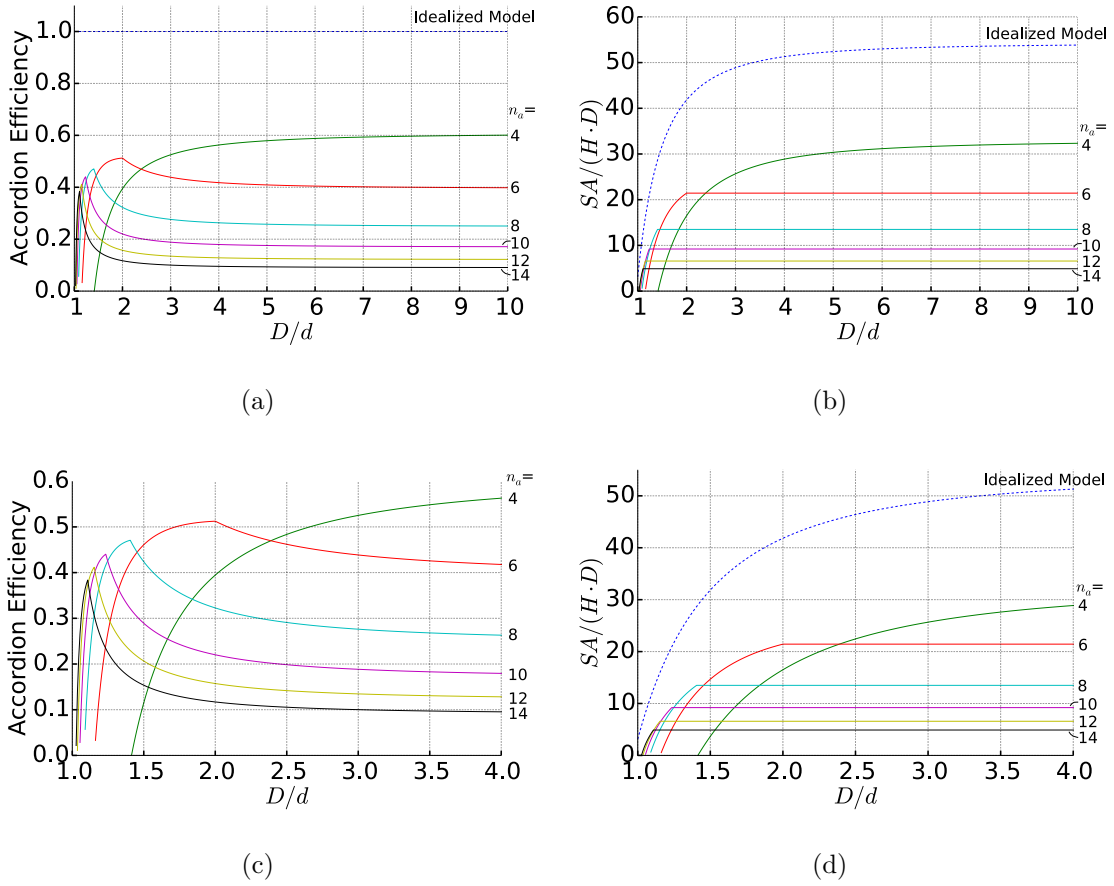

Figure 4.13: Efficiency (SA_k/SA_i) values over a range of D/d values for Accordion patterns with $n_a = 4, 6, 8, 10, 12, 14$.

rest of the range of D/d values) are tabulated in Table 4.3. Examining Fig. 4.13(c), each value of n_a has a range of D/d where it has the highest efficiency. Ranges of D/d where each value of n_a has the highest efficiency are tabulated in Table 4.3.

All of the patterns shown in Fig. 4.13 except $n_a = 4$ have a transition point and constant surface area and thus decreasing efficiency after some point as D/d is increased. This is because in each case at some point one of the side lengths could not be decreased below zero. A graphical method using panel reflection was used to consider one of these cases, shown in Fig. 4.14. In this plot, top-down transparencies are shown along with their associated D/d value at three points for an accordion with $n_a = 6$. At $D/d = 1.5$, the pattern matches the annulus and each side length is a finite, positive number. As D/d is increased to 2.0, one of the side lengths (c) decreases to zero but the pattern still matches

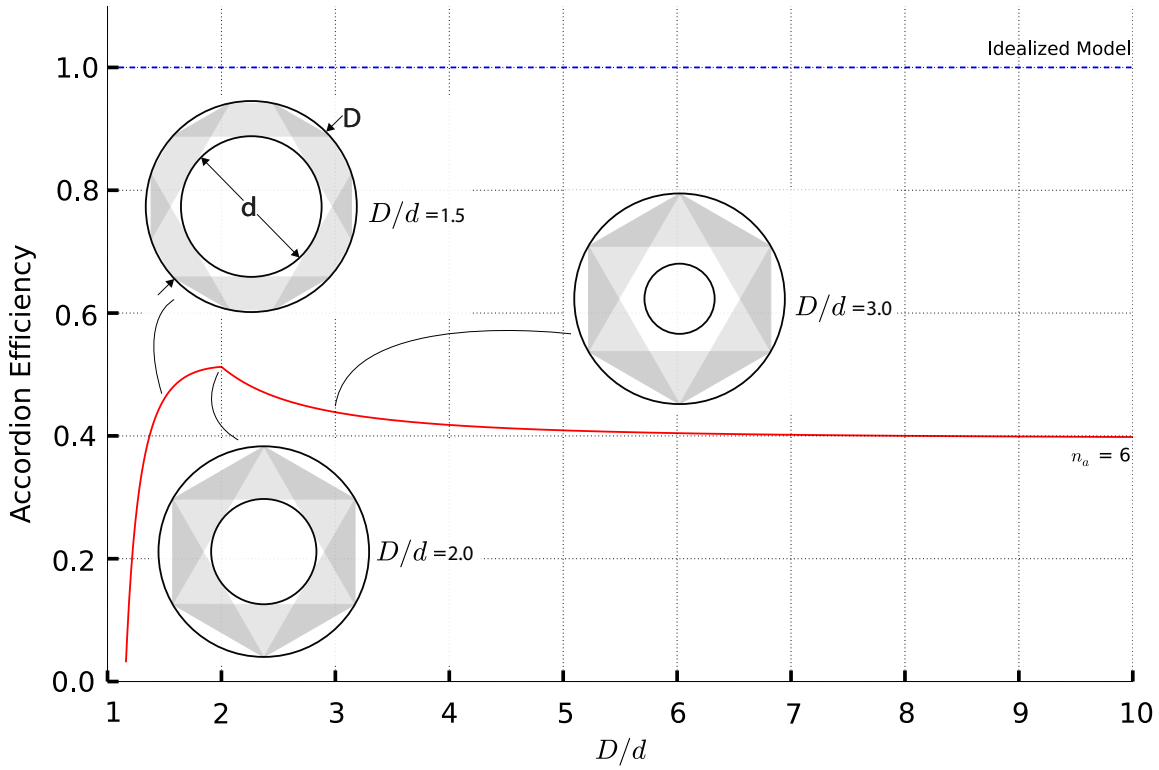

Figure 4.14: Top-down transparencies are shown along with their associated D/d value at three points for an accordion with $n_a = 6$. After the transition point at $D/d = 2.0$, surface area remains the same and thus efficiency decreases.

the annulus. At every D/d value greater than 2.0, pattern surface area cannot be increased because the c side length has reached a limit of 0. Thus, as D/d increases past the transition point, the pattern no longer matches the inner circle but can still be folded and fit within the annulus, and the efficiency decreases due to the surface area remaining the same. While each value of n_a has a different transition point, all but the $n_a = 4$ accordion experience this same phenomenon. The $n_a = 4$ accordion does not have a transition point because it can be formed with a d value of approximately 0.

Theoretical maximum efficiency for the pattern with $n_a = 4$ was verified by considering the case where $d = 0$ and the accordion pattern turns into a diamond pattern. An example with $D/d = 3$ is shown in Fig. 4.15(a). The value of D/d is increased to 20 in Fig. 4.15(b). In this case, the pattern approaches a diamond pattern with two layers stacked on top of each other. If we overlay two of the disks from the Idealized Model with these two

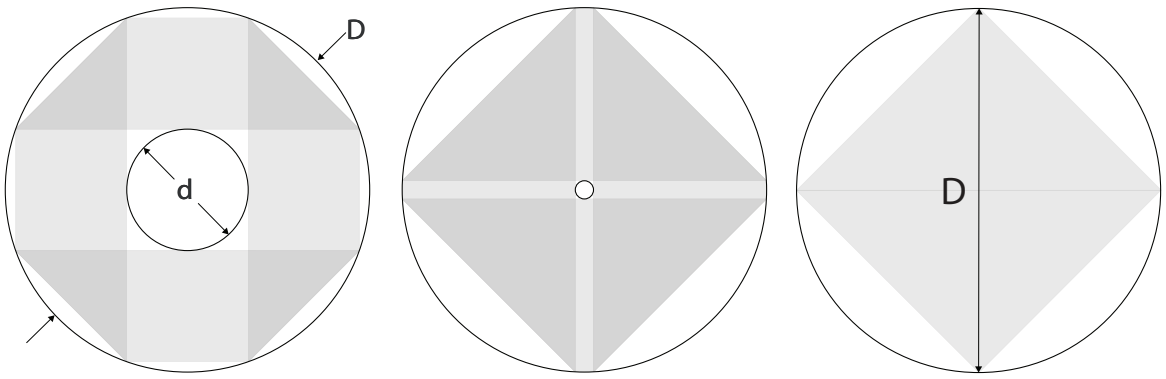

Figure 4.15: One layer of Accordion $n_a = 4$ flat fold transparency with (a) $D/d = 3$, (b) $D/d = 20$ (approaching theoretical limit of $d = 0$, note how it is approaching being two squares overlaid on each other), and (c) one square (one layer of the two squares) of theoretical limit with $D/d = 1000$ overlaid on one disk model disk with disk diameter and diagonal D labeled.

diamonds, we can see that a square is effectively laying on each of the disk model disks, with corner-to-corner distance of D, shown in Fig. 4.15(b). The surface area of each disk is $SA_{disk} = \pi D^2/4$ and the surface area of each diamond is $SA_{diamond} = D^2/2$, so the maximum theoretical amount of overlap should be close to $SA_{disk}/SA_{diamond} = 2/\pi = 0.63662$. Examining Fig. 4.13(a), as the ratio of D/d increases the theoretical surface area approaches this number, thus verifying the theoretical model. A model was created with $D/d = 100,000$, and the maximum value achieved by the Accordion with $n_a = 4$ was 0.6081, with the difference likely being due to the Idealized Model's cylinders between alternating layers.

Other GS/D values were considered at different D/d values to see if consistent results were achieved. A table considering peak efficiency values with GS/D ranging from 0.002 (observed in a commercial filter) to 0.03 is shown in Table 4.5. Examining this table, the value of GS/D at a specific D/d value has almost no impact in efficiency, which is likely due to how similar the Accordion is to the Idealized Model when its surfaces are horizontal. It should be noted that due to the discrete nature of the functions involved, sampling as has been done in this table results in some minor aliasing.

Table 4.3: Maximum efficiency and normalized surface area compared to D/d for Accordion patterns with $GS/D = 0.015$.

n_a	Maximum Efficiency	Maximum Normalized Surface Area	D/d
4	0.6008	32.3400	10.0000
6	0.5125	21.4341	2.0000
8	0.4708	13.4961	1.4054
10	0.4403	9.2089	1.2342
12	0.4117	6.5782	1.1532
14	0.3838	4.8926	1.1081

Table 4.4: D/d ratios for different values of n_a with maximum efficiency. Note that no Accordion can be created at $D/d = 1.0$, hence initial starting values are all higher than 1.0.

n_a	D/d Range
4	2.3964 - 10.000
6	1.4595 - 2.3964
8	1.2523 - 1.4595
10	1.1622 - 1.2523
12	1.1171 - 1.1622
14	1.0270 - 1.1171

Table 4.5: Accordion efficiency values for a range of GS/D and D/d values.

GS/D	D/d					
	1.5	2	2.5	3	3.5	4
0.002	0.0707	0.3183	0.4329	0.4951	0.5327	0.5570
0.010	0.0707	0.3183	0.4329	0.4951	0.5327	0.5570
0.015	0.0702	0.3159	0.4296	0.4914	0.5287	0.5529
0.020	0.0707	0.3183	0.4329	0.4951	0.5327	0.5570
0.025	0.0707	0.3183	0.4329	0.4951	0.5327	0.5570
0.030	0.0707	0.3183	0.4329	0.4951	0.5327	0.5570

4.6 Kresling design and comparison to Idealized Model

The Kresling pattern, a variation of the Yoshimura pattern [42,43] and also similar to a pattern previously called the Fujimoto pattern [44], is the final Origami-based cylindrical packing pattern considered here. Like the Accordion, it has been used previously as a bellows that can be expanded and contracted in the longitudinal direction [30]; its planes lie nearly horizontal when it is set on its end and compressed.

4.6.1 Kresling design parameters

The geometry of the Kresling pattern consists of a set of repeated triangles arranged in stacked parallelograms [45]. This pattern is a subset of the possible patterns created when triangulating a cylinder [46–48] where the a sides of the base unit are parallel with the ground, and extensive studies have been performed previously characterizing its properties [19,42,43]. A base tesselation unit composed of two triangles arranged into a parallelogram and its required variables a, b, c, and ϕ, is shown in Fig. 4.16(a). Inputs for the equations used to define the base unit include the interior diameter d and exterior diameter D of the annulus the pattern lies inside as well as n_k, the number of sides of the polygon forming the bottom of the folded Kresling. One form of the equations used to fully define the Kresling base tesselation unit is presented as shown in [30] as

$$\phi = \frac{\pi}{n_k} \tag{4.30}$$

$$a = D\sin(\phi) \tag{4.31}$$

$$b = D\sin\left(\arccos\left(\frac{d}{D}\right) - \phi\right) \tag{4.32}$$

$$c = D\sin\left(\arcsin\left(\frac{b}{D}\right) + \phi\right) \tag{4.33}$$

Parameter n_k defines how many base tesselation units are necessary to create a fully-functional cylindrical Kresling pattern, and n_k determines the number of sides of the base polygon on each Kresling layer. When determining n_k, an integer value greater than or

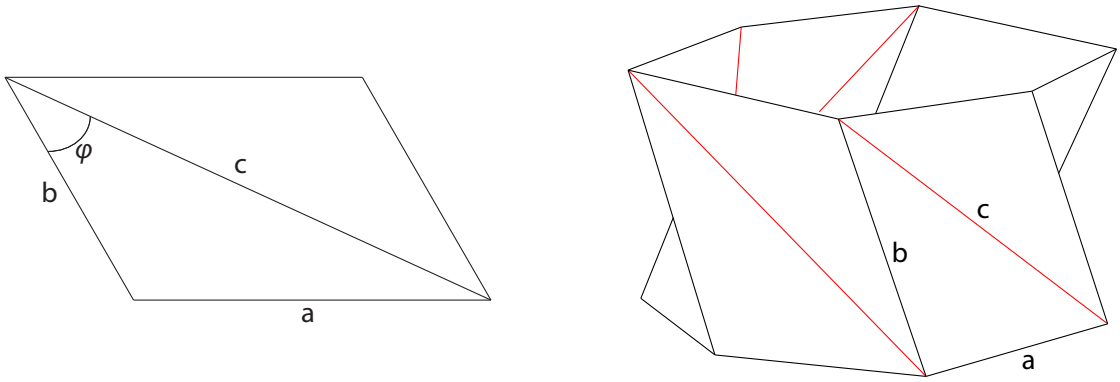

(a) (b)

Figure 4.16: (a) Kresling base unit and (b) $n_k = 6$ single layer wireframe.

equal to three must be chosen. As n_k is increased, the pattern will more closely approximate an annular shape, but after drastic improvement in surface area up to $n_k = 12$ there are diminishing returns in how well the shape matches an annulus and corresponding significant increases in manufacturing difficulty due to extra distinct folds. This parameter can either be chosen arbitrarily or allowed to change as part of an optimization routine with an objective function of maximizing surface area.

The final parameter used to fully define the flat pattern is s_k, the number of stories. The base tesselation units can be arrayed in either alternating directions for each story s_k or in the same direction, as shown in Fig. 4.17. This will affect the rotation of the unit as it deploys but not the ability of the unit to fold or its characteristics when compressed to some constant height. Because each story connects with each adjacent story with sharp, angular creases rather than squared off double pleats, the pattern must be modified to provide a more consistent comparison to the other fold patterns and theoretical model.

4.6.2 Kresling pattern modification

The Kresling pattern must be modified to have generally "u" shaped folds instead of "v" shaped folds. However, the method used for the Accordion pattern modification must be adapted to work for the Kresling pattern modification. When one vertex is considered independent of all other vertices in the pattern, layer ordering of planes from 1 to 6 in

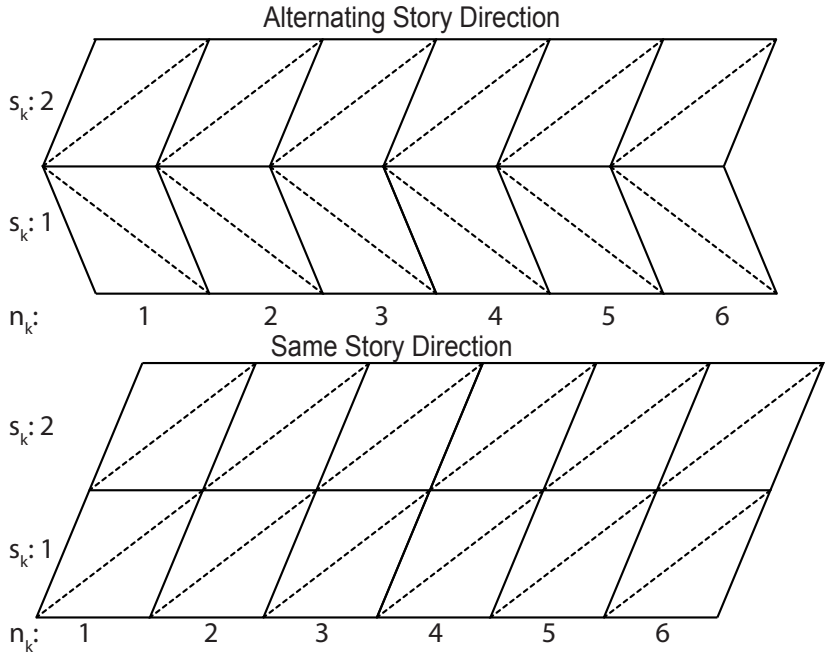

Figure 4.17: Kresling with $s_k = 2$ and $n_k = 6$ composed in alternating story direction and same story direction. These patterns will show different behavior when compressing and expanding (rotational behavior) but will be equivalent in surface area and overall dimensions. Mountain folds are solid lines and valley folds are dashed lines.

sequential stacking order and application of finding difference in panel number results in offsets of $1GS$ for each crease except for one where the panel 6 lies on top of the panel 1, resulting in an offset of $5GS$, shown in Fig. 4.18(a). However, as soon as multiple vertices are considered, conflicts in the offsets arise. Specifically, one vertex analysis specifies a gap of $5GS$ while the adjacent vertex analysis specifies a gap of $1GS$. To resolve this conflict, it was found that a tapered line between the two conflicting values resulted in a functional fold pattern, shown in Fig. 4.18(b). Photos of a prototype folded using this pattern are shown in Fig. 4.19. As is the case with the Accordion pattern, it should be noted that if the value of GS is too large, the overall diameter D of the actual prototype will be smaller than the desired D value. It is assumed that applications such as filters that might use this research will have a GS small enough to not present a major problem in this regard.

$$s_k = floor\left(\frac{H}{5GS}\right) \tag{4.34}$$

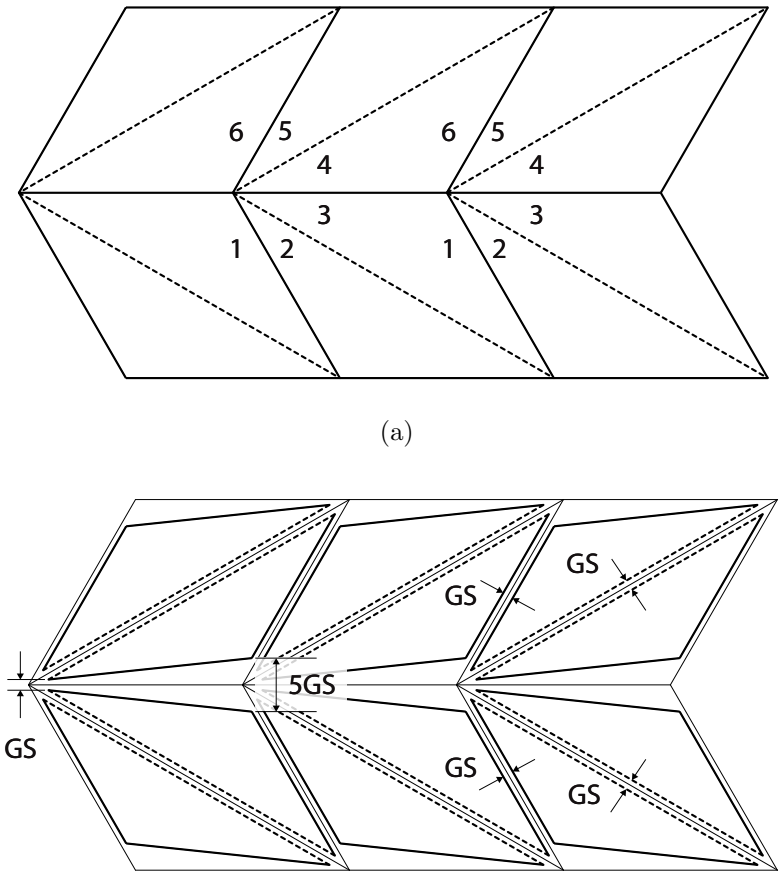

Figure 4.18: (a) Layer ordering of two adjacent Kresling vertices and (b) offset crease technique applied with taper from one vertex to the adjacent vertex. This portion of the Kresling pattern is a smaller portion of the diagram presented in Fig. 4.17 and these offsets are applied to the entire pattern before folding.

It must be noted that a traditional offset crease method involves removing material at the vertices. However, in this case as in the Accordion pattern, the material at the vertices cannot be removed but must be allowed to wrinkle and create "soft-creases" which behave unpredictably.

4.6.3 Kresling efficiency analysis

The equations presented can be used to design a wide range of Kresling patterns. Given a specified inner diameter d, outer diameter D, number of sides n_k, overall height H, and minimum gap size GS, the pattern can be fully generated. Surface area SA_k can then

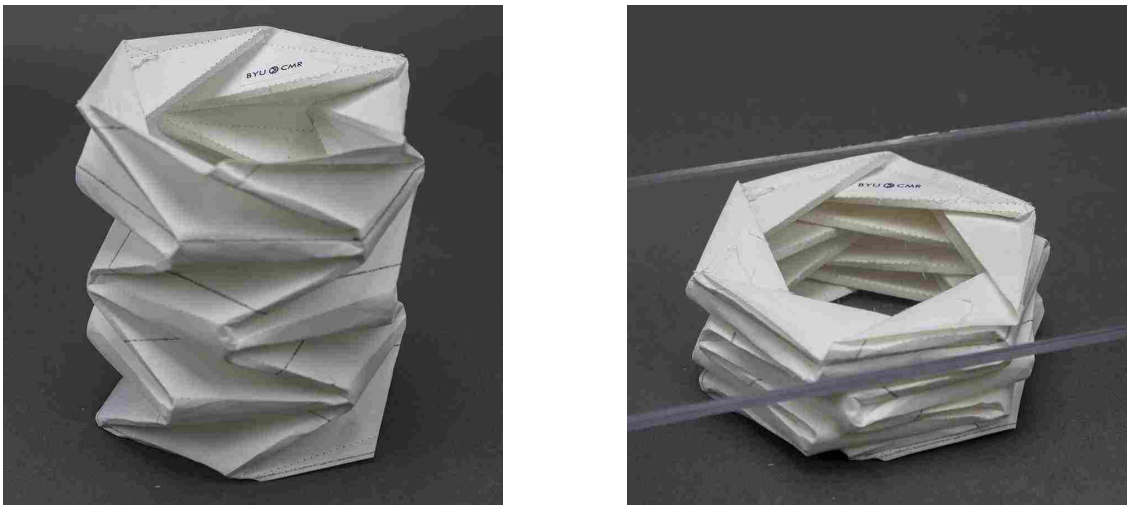

(a) (b)

Figure 4.19: Kresling prototype with $n_k = 6$ (a) uncompressed and (b) compressed.

be calculated as the surface area of the flat pattern, using Heron's formula for calculating surface area of a triangle using the three side lengths, multiplied by 2, n_k, and s_k to account for all tesselation units. Variable p is the semiperimeter of the base triangle.

$$p = \frac{1}{2}(a + b + c) \tag{4.35}$$

$$SA_k = 2n \cdot s_k \cdot \sqrt{p(p-a)(p-b)(p-c)} \tag{4.36}$$

These equations were used to generate a range of patterns to compare to the Idealized Model. It should be noted that while n_k can be either even or odd as long as it is greater than 3, even integers were arbitrarily chosen for this analysis. Similar to the Accordion, a primary point of interest is the effect of n_k on overall efficiency. A plot comparing efficiency for a range of n_k values and across a range of D/d values is shown in Fig. 4.20(a), and a plot considering surface area normalized by $H \cdot D$ is shown in Fig. 4.20(b). Maximum efficiency and normalized surface area values and associated D/d values are tabulated in Table 4.6. It can also be seen from this plot that increasing the value of n_k results in improved efficiency but at a diminishing rate of improvement. To further understand this phenomenon, a plot comparing efficiency for a pattern with a constant $D/d = 3$ as n_k is increased from 3 to 40 is

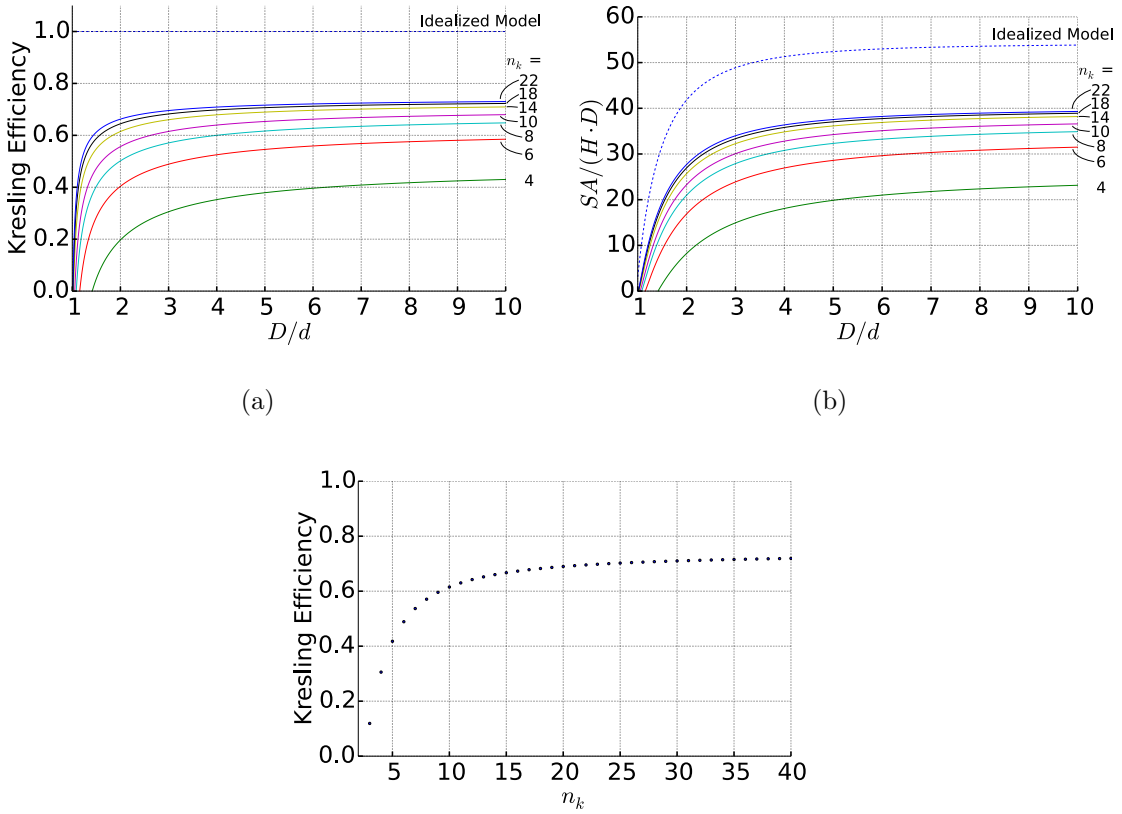

Figure 4.20: (a) Effect of n_k on efficiency (SA_k/SA_i) of Kresling pattern over range of D/d values for $GS/D = 0.015$ (b) normalized surface area of Kresling pattern and (b) Effect of n_k on efficiency for Kresling with $D/d = 3$.

shown in Fig. 4.20(c). After n_k passes approximately 10, the rate of improvement drastically decreases. The overall efficiency approached approximately 0.748 in an asymptotic fashion as n_k increased to 10000. As such, a designer must balance possible improvements with increased manufacturing complexity when designing Kresling patterns.

Other GS/D values have been considered at different D/d values to see if consistent results were achieved. A table considering peak efficiency values with GS/D ranging from 0.002 (observed in a commercial filter) to 0.03 for a Kresling with $n_k = 10$ is shown in Table 4.7. Examining this table, the value of GS/D at a specific D/d value has almost no impact in efficiency, which is, like the Accordion, likely due to how similar the Kresling is to the Idealized Model when its surfaces are nearly horizontal.

Table 4.6: Maximum efficiency ratios for Kresling patterns with various n_k values.

n_k	Maximum Kresling Efficiency	Maximum Normalized Surface Area	D/d
4	0.4301	23.1530	10
6	0.5851	31.4970	10
8	0.6481	34.8864	10
10	0.6797	36.5888	10
14	0.7095	38.1919	10
18	0.7229	38.9141	10
22	0.7302	39.3085	10

Table 4.7: Kresling efficiency values for a range of GS/D and D/d values.

GS/D	D/d					
	1.5	2	2.5	3	3.5	4
0.002	0.5241	0.6026	0.6374	0.6578	0.6715	0.6813
0.010	0.4985	0.5818	0.6186	0.6400	0.6543	0.6646
0.015	0.4728	0.5566	0.5935	0.6151	0.6294	0.6396
0.020	0.4698	0.5578	0.5965	0.6191	0.6340	0.6448
0.025	0.4567	0.5465	0.5861	0.6091	0.6244	0.6353
0.030	0.4375	0.5275	0.5672	0.5903	0.6056	0.6166

4.7 Discussion

All patterns have been compared and the results are plotted in Fig. 4.21, using 1000 data points for each pattern, over a range of D/d from 1.0 to 10.0 and with $GS/D = 0.015$. Both the Basic and M-pleats have $IGS = T_p = GS$. The Basic Pleat, M-pleat, and Accordion composite line are plotted with their maximum possible value at every D/d value. For each of these patterns the highest overall surface area can be used at ranges of D/d where the patterns lie within the annulus but do not necessarily match both the inner and outer circles, similar to the approach taken with the Accordion pattern shown in Fig. 4.14. For the Accordion pattern, the line plotted is a composite of the best performance from the various n_a values used in Fig. 4.13(a). Table 4.4 can be used to determine which n_a is used for different portions of the line. The Kresling pattern compared had $n_k = 10$, as this is a good balance between manufacturability (physically possible to fold) and high efficiency (from Fig. 4.20(c)), but other values could be chosen which would shift this line up or down respectively.

Analyzing the results, the Basic Pleat and M-pleat have significantly higher efficiency at low ranges of D/d. They are within 10% of the same value from $D/d = 1.00$ to 1.5135, at which point the M-pleat begins to have significantly better efficiency. Peak normalized surface area values for each pattern and associated D/d values are shown in Table 4.8. As the ratio of D/d increases, both the Basic Pleat and M-pleat decrease in efficiency after they peak. If the only concern is that the pattern fit within the annulus described by D/d, and not necessarily match the inner diameter, the parameters from the highest efficiency point could be held constant and used for every D/d after that point, similar to the method used with the Accordion pattern (and shown in Fig. 4.14). Fig. 4.21(b) shows the normalized surface area.

The Accordion and Kresling do not ever reach the efficiency of the M-pleat, but they can be used at very high ratios of D/d and match both the outer and inner diameters with no decrease in efficiency, while the M-pleat does not match the inner diameter d after its peak value, and has been found to be difficult to implement in practice [36].

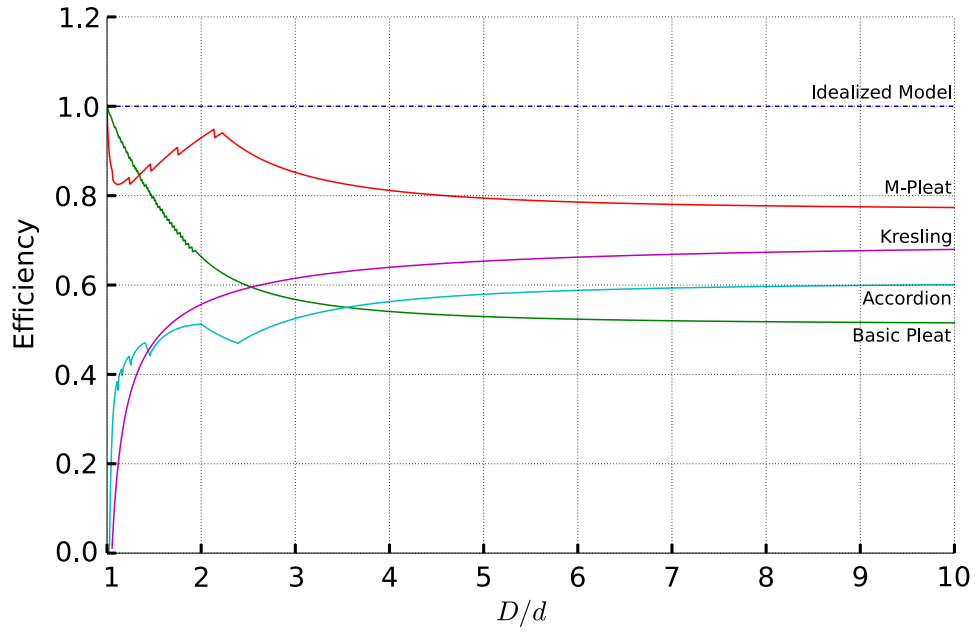

(a)

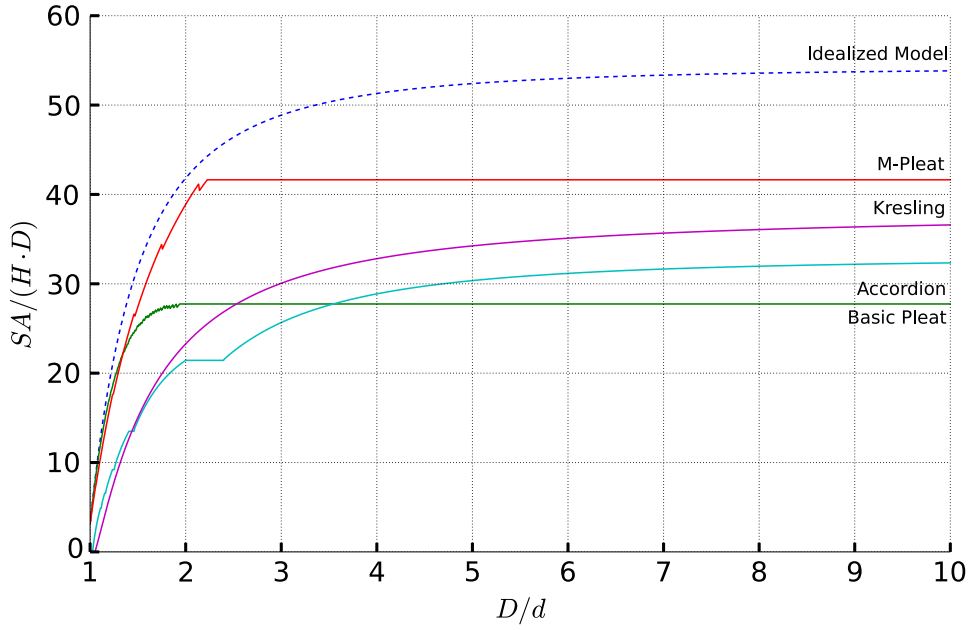

(b)

Figure 4.21: (a) Overall efficiency (SA/SA_i) comparison with $GS/D = 0.015$ over range of D/d values from 1.00 to 10. The Kresling pattern has $n_k = 10$ while the Accordion pattern is a composite of the best efficiency based on different values of n_a. (b) Normalized surface area for each pattern.

These results can be used to determine which pattern is most desirable over ranges of D/d, presented in Table 4.9. The Basic Pleat has the highest value for a short range and the M-pleat then has the highest value over the remaining values of D/d. However, there are other considerations that must be made when determining which pattern to use.

Although this chapter considers the efficiency of patterns, efficiency is only one of many considerations to be made when selecting a fold pattern for a filter design. Results of flow testing would be required to validate mathematical model assumptions and pattern modifications, thus verifying or adjusting the resulting graphs and tables. Vertical stability could also be considered. Patterns such as the Basic Pleat and M-pleat have surfaces aligned with the longitudinal axis of the cylinder and are rigid in that direction, while Origami-based patterns such as the Accordion and Kresling have surfaces primarily in the horizontal direction (transverse to the longitudinal axis). This results in potential vertical expansion and compression, which could have adverse effects due to vibration but could also be utilized to allow for dynamic filter behavior. In addition, ease of manufacturing could also be considered when determining which pattern to use. Existing processes work well for pleats such as the Basic Pleat and M-pleat, but new processes utilizing mechanisms including rollers would need to be developed to allow for efficient manufacturing of complex origami-based filters.

Table 4.8: Max SA/SA_i Ratios, $GS/D = 0.015$, all patterns.

Pattern	Maximum Normalized Surface Area	D/d
Basic Pleat	27.7429	≥ 1.9369
M-Pleat	41.6378	≥ 2.2236
Accordion	15.4081	10.000
Kresling	22.5336	10.000

Table 4.9: D/d ratios for fold patterns with maximum efficiency.

Pattern	D/d Range
Basic Pleat	1.00 - 1.3514
M-pleat	1.3514 - 10.00

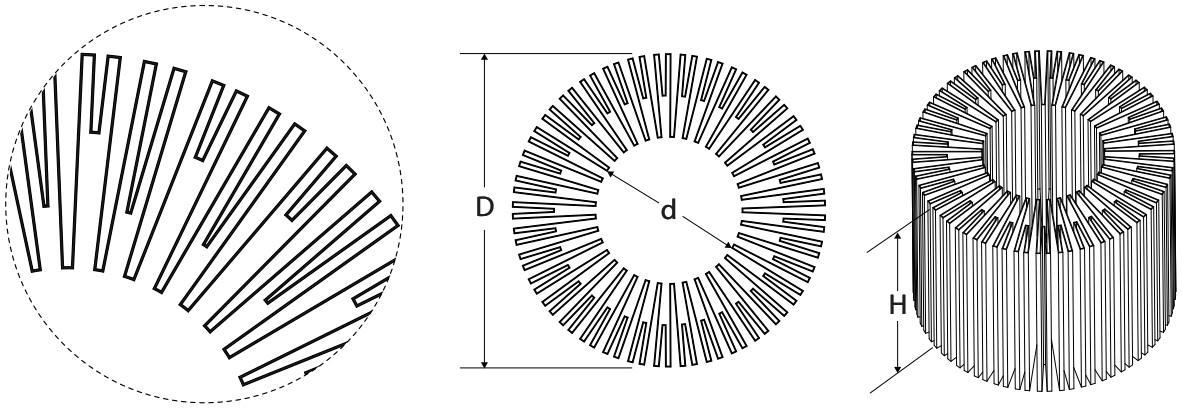

(a) (b)

Figure 4.22: (a) M-pleat with uneven short pleats top and angled views and (b) zoomed view of M-pleat with uneven short pleats.

Finally, many fold pattern variations exist as possible solutions beyond the four presented here. For example, a pattern could be generated as a variation of the M-pleat with unequal pleat lengths. An example where M-pleats have two alternate lengths is shown in Fig. 4.22(a) and Fig. 4.22(b). Further work could be pursued to analyze such a pattern, and many other patterns could also be considered by designers in addition to those analyzed here.

4.8 Conclusion

The objective of analyzing multiple patterns that are conducive to packing a large amount of area into an annular cylinder was accomplished. Geometric analysis relative to a Idealized Model was presented and discussed for four patterns including the Basic Pleat, M-pleat, Accordion, and Kresling. It was found that based purely on geometry the M-pleat provides the highest overall efficiency for a large range of D/d values while the Basic Pleat has the highest efficiency over a small range of D/d. Detailed initial analysis of each pattern showed interesting behavior and a variety of efficiencies based on physical parameters. Physical prototypes were created for multiple patterns, and the equations presented here can be used to design a large variety of patterns that fit within cylindrical volumes.

CHAPTER 5. CONCLUSION

5.1 Conclusion

In conclusion, the objective of this research was met. New methods and metrics for configuring packed prisms using Origami-based methods including Soft Origami and traditional Origami were presented, examined, and applied. Conclusions based on each of the chapters are as follows:

1. Soft Origami provides a viable method for packing soft-sheet materials into fully-dense cylindrical volumes. Depending on the application requirements (i.e. if the pattern is to be deployed via internal pressure or some other method; if the resulting deployment requires spin or not, etc.), an existing Origami pattern can likely be found that results in a fully-dense cylinder that performs in an acceptable manner. When applying Soft Origami patterns, unlike in traditional Origami, the method of application (packing method) has equal importance for deployment performance as does the pattern chosen. This was shown by the demonstrated application to automotive airbags. A key point of this approach is that many packing methods may need to be explored to find the best option.

2. The ninety-degree special case of the Miura-ori can be used to pack continuous arbitrary-shaped sheet materials into a wide range of fully-dense arbitrary prisms. This method could be used on soft-sheet materials as well, and provides a highly customizable method for packing sheet materials into specific shapes. Similar patterns have been used in the past for map folding and mechanism design. However, this method provides a new, simple way to configure fully-dense arbitrary prisms, and could have an impact in fields where a soft-sheet material needs to be packed into a specific prismatic shape. Because of its potential applicability to soft materials, this method could be

considered a combination of a traditional Origami method (ninety-degree Miura Ori) with Soft Origami applications.

3. Comparisons can be made between traditional (industry-accepted) and Origami-based patterns that pack large amounts of surface area into annular cylinders based on efficiency given specific overall dimensions. Objective comparison is best done by using an idealized high-surface-area model and by modifying patterns in ways that provide equal spacing between layers, although other factors must also be considered when determining which patterns to use. Geometric analysis such as this can be a useful starting point for designing for applications such as fluid filters, and using both traditional (industry-accepted) and Origami patterns provide a useful comparison of established patterns and new patterns.

5.2 Future Work

Future work could be done to elaborate and expand the research shown here including the following:

1. Other applications beside the airbag application shown in Chapter 2 could be considered where soft-sheet materials need folded into cylinders. In particular, the Flasher pattern was not well-suited to airbag application, but other applications for this pattern where rotation is not a concern could be examined.

2. "Origami tooling" could be explored as a means for folding soft-sheet materials and sheet materials into Origami patterns. Using Origami to make Origami (as was done when applying the Flasher pattern to airbags using an Origami folding table) would be valuable for both applications where the origami pattern is permanently imprinted on the soft-sheet-material and applications where it is temporarily imprinted (i.e. permanent creases are not formed, such as in automotive airbags).

3. Fully-dense arbitrary prism packing shown in Chapter 3 with the ninety-degree Miura-ori could be extended to arbitrary three-dimensional shapes by using reverse folds to change the orientation of the packed shape, which could have application in industries

where 3-D shapes are used to support fragile items. A possible application could be making a support material for shipping that can start as a flat sheet (e.g. cardboard) and fold into a shape for shipping fragile items, potentially replacing non-eco-friendly packing materials such as packing peanuts and styrofoam packing materials with packing materials that can be recycled. Thickness-accomodation methods for when the material is not a soft-sheet material would also be particularly useful when folding patterns with high numbers of vertical grid lines.

4. Further testing and refinement in collaboration with a fluid filter company would be invaluable to determine whether assumptions made about necessary pleat spacing were valid in Chapter 4 and to further refine comparisons made. Adding experimental data to the geometric analysis would provide the necessary knowledge to apply the origami patterns discussed to engineering applications.

Finally, other methods for configuring cylinders and prisms that are either fully-dense and partially-dense should be explored and applied in practice to allow designers in various fields the ability to quickly generate patterns and methods for specific applications.

REFERENCES

[1] T. Tachi, "Rigid-Foldable Thick Origami," *Origami 5 Fifth International Meeting of Origami Science Mathematics and Education*, pp. 253–264, 2011. 4, 36

[2] B. J. Edmondson, R. J. Lang, and L. L. Howell, "An Offset Panel Technique for Thick Rigidly Foldable Origami," in *Proceedings of the ASME 2014 International Design Engineering Technical Conferences & Computers and Information in Engineering Conference*, Buffalo, New York, 2014. 4, 36

[3] T. A. Evans, R. J. Lang, S. P. Magleby, and L. L. Howell, "Rigidly foldable origami gadgets and tessellations," *Royal Society Open Science*, vol. 2, no. 9, Sep. 2015. 4

[4] S. A. Zirbel, R. J. Lang, M. W. Thomson, D. A. Sigel, P. E. Walkemeyer, B. P. Trease, S. P. Magleby, and L. L. Howell, "Accommodating Thickness in Origami-Based Deployable Arrays," *Journal of Mechanical Design*, vol. 135, no. 11, p. 111005, 2013. 4, 5, 10, 33, 37

[5] T. G. Nelson, R. J. Lang, S. P. Magleby, and L. L. Howell, "Large-Curvature Deployable Developable Structures via Lamina Emergent Arrays," in *ASME 2015 International Design Engineering Technical Conferences & Computers and Information in Engineering Conference*, Boston, Massachusetts, 2015. 4, 8

[6] R. D. Koschitz, "Computational Design with Curved Creases: David Huffmanś Approach to Paperfolding," Ph.D. dissertation, Massachusetts Institute of Technology, 2014. 4, 11

[7] J. M. Gattas and Z. You, "Miura-Base Rigid Origami: Parametrizations of Curved-Crease Geometries," *Journal of Mechanical Design*, vol. 136, no. 12, p. 121404, 2014. 4, 27

[8] R. J. Lang, "Computational origami: From flapping birds to space telescopes," in *Twenty-fifth Annual Symposium on Computational Geometry*, Hershberger and E. Fogel, Eds. New York, NY, USA: ACM, 2009, pp. 159–162. 4

[9] T. Tachi, "Origamizing polyhedral surfaces," *IEEE Transactions on Visualization and Computer Graphics*, 2010. 4

[10] J. Morgan, R. J. Lang, S. P. Magleby, and L. L. Howell, "A Preliminary Process For Origami-Adapted Design," in *ASME 2015 International Design Engineering Technical Conferences & Computers and Information in Engineering Conference*, Boston, Massachusetts, 2015. 4, 36

[11] K. Kuribayashi, K. Tsuchiya, Z. You, D. Tomus, M. Umemoto, T. Ito, and M. Sasaki, "Self-deployable origami stent grafts as a biomedical application of Ni-rich TiNi shape memory alloy foil," *Materials Science and Engineering: A*, vol. 419, no. 1-2, pp. 131–137, 2006. 5

[12] C. T. Klodell Jr, J. M. Aranda, D. C. McGiffin, B. K. Rayburn, B. Sun, W. T. Abraham, W. E. Pae, J. P. Boehmer, H. Klein, and C. Huth, "Worldwide surgical experience with the Paracor HeartNet cardiac restraint device," *Journal of Thoracic and Cardiovascular Surgery*, vol. 135, no. 1, pp. 188–195, 2008. 5

[13] C. M. Wheeler and M. L. Culpepper, "Soft Origami: Classification, Constraint, and Actuation of Highly Compliant Origami Structures," *Journal of Mechanisms and Robotics*, 2015. 5

[14] T. C. Taylor, "Inflatable habitation volumes in space," U.S. Patent 6 439 508, August, 2002. 5

[15] R. T. Bigelow, "Emergency safe haven," U.S. Patent 20 060 005 474, January, 2006. 5

[16] R. T. Bigelow, "Inflatable satellite bus," U.S. Patent 6 962 310, November, 2005. 5

[17] E. H. J. Ingham, "Inflatable airlock," U.S. Patent 20 120 318 926, December, 2012. 5

[18] J. M. Gattas, W. Wu, and Z. You, "Miura-base rigid origami: parameterizations of first-level derivative and piecewise geometries," *Journal of Mechanical Design*, vol. 135, no. 11, p. 111011, 2013. 8

[19] C. Jianguo, D. Xiaowei, Z. Ya, F. Jian, and T. Yongming, "Bistable Behavior of the Cylindrical Origami Structure With Kresling Pattern," *Journal of Mechanical Design*, vol. 137, no. 6, p. 061406, 2015. 8, 58

[20] B. H. Hanna, J. M. Lund, R. J. Lang, S. P. Magleby, and L. L. Howell, "Waterbomb base: a symmetric single-vertex bistable origami mechanism," *Smart Materials and Structures*, vol. 23, no. 9, p. 094009, 2014. 8

[21] R. J. Lang, S. P. Magleby, and L. L. Howell, "Single Degree-of-Freedom Rigidly Foldable Cut Origami Flashers," *Journal of Mechanisms and Robotics*, vol. 8, 2016. 8

[22] J. Mitani and T. Igarashi, "Interactive Design of Planar Curved Folding by Reflection," in *Pacific Graphics*, B.-Y. Chen, J. Kautz, T.-Y. Lee, and M. C. Lin, Eds., Kaohsiung, Taiwan, 2011. 8

[23] E. D. Demaine and M. L. Demaine, "Curved Crease Folding a Review on Art , Design and Mathematics Curved Creases in Art and Design," *Proceedings of the IABSE-IASS Symposium: Taller, Longer, Lighter (IABSE-IASS 2011)*, 2011. 8

[24] E. D. Demaine, M. L. Demaine, and D. Koschitz, "Reconstructing David Huffmans Legacy in Curved-Crease Folding," in *Origami5: Proceedings of the 5th International Conference on Origami in Science, Mathematics and Education*, 2011, pp. 39–52. 10

[25] R. J. Lang, "One Ellipse to Rule Them All," *Origami USA*, 2013. 11

[26] K. Miura, "Method of Packaging and Deployment of Large Membranes in Space," 1985. 27

[27] C. Hoberman, "Curved Pleated Sheet Structures," U.S. Patent 5 234 727, 1993, Patent 5,234,727. 27

[28] C. Hoberman, "Reversibly expandable structures," U.S. Patent 4 981 732, 1991, US Patent 4,981,732. 33

[29] C. Hoberman, "Folding Structures Made of Thick Hinged Sheets," U.S. Patent 7 794 019, 2010. 33

[30] J. Butler, J. Morgan, N. Pehrson, K. Tolman, T. Bateman, S. P. Magleby, and L. L. Howell, "Highly Compressible Origami Bellows For Harsh Environments," in *ASME 2016 International Design Engineering Technical Conferences & Computers and Information in Engineering Conference*, 2016. 34, 49, 58

[31] T. Hartmann, "Corrugated fluid treatment packs and methods of making them," U.S. Patent 8 236 210, 2012. 36

[32] R. C. Stoyell, K. M. Williamson, S. D. Hopkins, and S. A. Geibel, "Filter," U.S. Patent 6 113 784, 2000. 36

[33] M. Schenk, A. D. Viquerat, K. a. Seffen, and S. D. Guest, "Review of Inflatable Booms for Deployable Space Structures: Packing and Rigidization," *Journal of Spacecraft and Rockets*, vol. 51, no. 3, pp. 762–778, 2014. 37

[34] E. T. Filipov, G. H. Paulino, and T. Tachi, "Origami tubes with reconfigurable polygonal cross-sections," *Proceedings of the Royal Society A: Mathematical, Physical and Engineering Science*, vol. 472, no. 2185, 2016. 37

[35] E. A. Janikowski, J. E. Dorgan, C. E. Holm, and Z. G. Liu, "High capacity direct flow filter with maintained channel width," U.S. Patent 7 323 105, 2008. 40

[36] K. E. Buckman and K. A. Rogers, "Fluid filter elements," U.S. Patent 3 799 354, 1974. 44, 46, 65

[37] R. De Magondeau, "Accordion pleated filter and method for making," U.S. Patent 2 732 951, 1956. 49

[38] R. H. Peyton and H. M. Misturado, "Accordion pleated fluid filtering element," U.S. Patent 4 936 991, 1990. 49

[39] M. Z. Patel, J. C. Taylor, and G. W. Schukar, "Fluid filter," U.S. Patent 7 981 184, 2011. 49

[40] N. R. Kane, "Mathematically optimized family of ultra low distortion bellow fold patterns," U.S. Patent 6 054 194, 2000. 49

[41] J. S. Ku and E. D. Demaine, "Folding Flat Crease Patterns with Thick Materials," *ASME 2015 International Design Engineering Technical Conferences & Computers and Information in Engineering Conference*, vol. 8, no. c, pp. DETC2015–48 039, 2015. 51

[42] Y. Yoshimura, "On the mechanism of buckling of a circular cylindrical shell under axial compression," Tech. Rep., 1955. 58

[43] K. Miura, "Proposition of Pseudo-Cylindrical Concave Polyhedral Shells," in *IASS Symposium on Folded Plates and Prismatic Structures*, 1970. 58

[44] S. Fujimoto, *Rittai Origami*. Osaka, Japan: Sinzo Kitigawa, 1970. 58

[45] B. Kresling, "Origami-structures in nature: lessons in designing "smart" materials," in *Materials Research Society Symposium*, 2012, pp. 42–54. 58

[46] S. D. Guest and S. Pellegrino, "The folding of triangulated cylinders, part I: geometric considerations," *Journal of Applied Mechanics*, vol. 61, no. 4, pp. 773–777, 1994. 58

[47] S. D. Guest and S. Pellegrino, "The folding of triangulated cylinders, part II: the folding process," *Journal of Applied Mechanics*, vol. 61, no. 4, pp. 778–783, 1994. 58

[48] S. D. Guest and S. Pellegrino, "The folding of triangulated cylinders, part III: the folding process," *Journal of Applied Mechanics*, vol. 63, no. 1, pp. 77–83, 1996. 58